

Do Tides Destabilize Trojan Exoplanets?

Anthony R. Dobrovolskis
SETI Institute
245-3 NASA Ames Research Center
Moffett Field, CA 94035-1000
Email: anthony.r.dobrovolskis@nasa.gov

Jack J. Lissauer [0000-0001-6513-1659]
Space Science & Astrobiology Division
245-3 NASA Ames Research Center
Moffett Field, CA 94035-1000

2022 April 28

37 pages

9 figures (including 1 with color)

4 tables

Proposed running head:

Do Tides Destabilize Trojan Exoplanets?

Correspondence:

Anthony R. Dobrovolskis
245-3 NASA Ames Research Center
Moffett Field CA 94035-1000
anthony.r.dobrovolskis@nasa.gov
Mobile: (669) 290-3437

Key Words:

Celestial mechanics

Extra-solar planets

Planetary dynamics

Tides, solid body

Resonances, orbital

HIGHLIGHTS

- Tides may prevent the survival of co-orbital exoplanets
- We generalize the theory of tides to include interactions among multiple perturbers
- We solve analytically for the motion of Trojan planets with tides
- We find that tidal dissipation pumps up small tadpole librations exponentially
- Our numerical simulations verify that tides remove Trojan planets

ABSTRACT

One outstanding problem in extrasolar planet studies is why no co-orbital exoplanets have been found, despite numerous searches among the many known planetary systems, many of them in other mean-motion resonances. Here we examine the hypothesis that dissipation of energy by tides in Trojan planets is preventing their survival.

The Appendix of this paper generalizes the conventional theory of tides to include tidal forces independent of dissipation, as well as the effects of one body on tides raised by another. The main text applies this theory to a model system consisting of a primary of stellar mass, a secondary of sub-stellar mass in a circular orbit about the primary, and a much lighter Trojan planet librating with small amplitude about an equilateral point of the system.

Next, we linearize the equations of motion about the Trojan points, including the tidal forces, and solve for the motion of the Trojan. The results indicate that tides damp out the Trojan’s motion perpendicular to the orbital plane of the primary and secondary, as well as its epicycles due to its eccentricity; but they pump up the amplitude of its tadpole librations exponentially. We then verify our analytic solutions by integrating the non-linearized equations of motion numerically for several sample cases. In each case, we find that the librations grow until the Trojan escapes its libration, which leads to a close encounter with either the primary or the secondary.

1 Introduction

Our Solar System contains numerous examples of “co-orbitals”, that is, objects sharing nearly the same orbital period about the same primary. The best known are the several thousand Trojan asteroids librating in “tadpole” orbits about either of Jupiter’s equilateral Lagrange points, like twin Sargassos of space; but Neptune also has numerous Trojan companions which are stable for Gyr timescales (*e.g.*, Sheppard and Trujillo, 2006). Small numbers of Trojans, all with large-amplitude librations, have been found for the planets Uranus, Mars, Earth, and Venus as well; but the orbits of these bodies are relatively short-lived, and imply that their occupants were captured into libration relatively recently in Solar System history.

In addition, each of Saturn’s moons Tethys and Dione has one small satellite at its leading Lagrange point L4, and another at its trailing Lagrange point L5. In the Circular Restricted Three-Body Problem (CR3BP), Trojans are stable for ratios M_1/M_2 of the primary mass to the secondary mass greater than $2/(1 - \sqrt{23/27}) = (27 + \sqrt{23 \times 27})/2 \approx 25.9599$ (*e.g.*, Dobrovolskis, 2013); for example, Pluto’s moon Charon, with $M_1/M_2 \approx 8.2$, cannot have Trojan companions.

Besides Trojans in tadpole orbits, other types of co-orbital companions are possible as well. For example, Saturn’s small moons Janus and Epimetheus are in a “horseshoe” resonance, such that Epimetheus librates about a wide arc enclosing both Janus’ L4 and L5 points. Horse-shoe resonances are stable for mass ratios $M_1/M_2 \gg 1200$ (Ćuk *et al.*, 2012); for example, with $M_1/M_2 \approx 3499$, Saturn could support long-term horseshoe companions, while with $M_1/M_2 \approx 1047$, Jupiter is not expected to have any.

“Quasi-satellites” appear to orbit a moon or planet in the retrograde direction (contrary to its orbital motion) and outside its Hill sphere (sometimes called its sphere of influence); but they are really in eccentric prograde orbits about the primary. Several quasi-satellites of Venus, Earth, and Neptune are known. In the CR3BP, quasi-satellites are stable for $M_1/M_2 \gg 21.0$ (Hénon and Guyot, 1970).

Furthermore, numerous asteroids are in hybrid co-orbital resonances, which alternate among tadpole, horseshoe, and quasi-satellite states. The Earth quasi-satellite 469219 Kamo’oalewa (a.k.a. 2016 HO3) is of this type, and is the target of a planned sample return mission by the China National Space Administration.

Finally, “counter-orbital” resonances are possible, when two objects orbit with the same period, but in opposite directions (Dobrovolskis, 2012; Morais & Namouni, 2013, 2016). To date only one counter-orbital companion of Jupiter has been found (Wiegert *et al.*, 2017): asteroid 2015 BZ 509, also known as (514107) Ka’epaoka’awela. Counter-orbitals seem to be stable for mass ratios $M_1/M_2 > \sim 7$; so even Charon could support counter-orbitals (Dobrovolskis, 2012).

In the past three decades, several thousands of extra-solar planets have been discovered and confirmed (*e.g.*, Rowe *et al.*, 2014; Guerrero *et al.*, 2021), including hundreds of multi-planet systems, several of them with resonances among their orbital periods (Lissauer *et al.*, 2011). Yet despite numerous directed searches for satellites or Trojan companions of exoplanets (*e.g.*, Caton *et al.*, 1999; Davis *et al.*, 2001; Ford & Gaudi, 2006; Ford & Holman, 2007; Narita *et al.*, 2007; Madhusudhan & Winn, 2009; Janson, 2013; Lillo-Box *et al.*, 2018a, 2018b; Kipping, 2020), not one exomoon or co-orbital exoplanet has yet been found.

Hipke & Angerhausen (2015) searched for statistical evidence for Trojan companions by stacking lightcurves of ~ 4000 *Kepler* planet candidates. They did not find evidence for such Trojans in their bulk analysis of the entire population; but they claimed a statistically significant detection of a Trojan population in the sub-sample of planet candidates with periods exceeding 60 days.

It remains a puzzle that no co-orbital exoplanets have been found yet, so some physics may well be preventing their formation, survival, or detection. Although our own Solar System contains no Trojan planets, theories of planet formation often predict that extrasolar planets should be accompanied by Trojan companions (*e.g.*, Laughlin & Chambers, 2002; Nauenberg, 2002; Goździewski & Konacki, 2006; Beaugé *et al.*, 2007; Giuppone *et al.*, 2012). Shared orbital periods can cause misinterpretation of astrometry and radial velocity signals, but usually should not confuse transit signatures and prevent detection (Dobrovolskis, 2013, 2015). Therefore we suspect that Trojan exoplanets may be unstable, on timescales shorter than the ages of most of the exoplanets identified by *Kepler*, *TESS*, and ground-based transiting planet searches.

The most likely explanation for the lack of confirmed moons of extrasolar planets is that they raise tides in their parent planets which drive evolution of the moon’s orbits, and ultimately destabilize most such exomoons large enough to be observable. Similarly, it is possible that tides raised by the primary star in Trojan exoplanets may destabilize their orbits. See Ferraz-Mello (2022) for a recent review of tidal effects on exoplanets in the two-body case.

In the two-body case, when the secondary already has been tidally despun to synchronous rotation, tides in the secondary always damp both its orbital eccentricity and semi-major axis (*e.g.*, Murray & Dermott, 1999). In the classic CR3BP, the equilateral Lagrange points L4 and L5 are known to be maxima of the energy integral (*e.g.*, Murray & Dermott, 1999). Thus it is plausible that energy dissipation may increase the amplitude of tadpole librations, and ultimately may destabilize Trojan orbits.

Many papers have addressed the effects of various types of dissipation on Trojans in our Solar System, such as drag by nebular gas and dust (Jeffreys, 1929; Greenberg, 1978; Yoder, 1979; Peale, 1993; Murray, 1994; Leleu *et al.*, 2019), radiation pressure and its associated Poynting-Robinson drag (Colombo *et al.*, 1966; Schuerman, 1980; Simmons *et al.*, 1985), and even torques from planetary rings (Lissauer *et al.*, 1985). These studies show that energy dissipation can either damp or pump orbital eccentricity and libration, depending on the particular functional form of the drag (Yoder *et al.*, 1983; Murray, 1994).

However, the Trojan problem with tidal dissipation in the third body has been treated very little. Caudal (2013) found that tides raised by Saturn on Janus and Epimetheus tend to de-stabilize their mutual horseshoe orbit; but that torques from Saturn’s rings tend to stabilize it, so that they may be evolving toward mutual tadpole orbits. In the same year, Rodríguez *et al.* (2013) used Mignard’s (1979) formulation of viscous-type tides numerically to integrate the planar motion of Trojan pairs with equal masses, and found them unstable to collision in every case.

Recently, Couturier *et al.* (2021) have used a Hamiltonian formulation of the planar problem to reach similar conclusions. An even more recent preprint by the same authors (Couturier *et al.*, 2022) finds that yet another massive planet, exterior to the co-orbitals but in mean-motion resonance with both of them, may significantly delay the onset of this instability, but cannot prevent it. This is intriguing because planets on nearby orbits typically destabilize co-orbital companions, as is the case for Trojan asteroids of Saturn (de la Barre *et al.*, 1996) and for multiple co-orbital planets on closely-spaced nested orbits (Smith and Lissauer, 2010).

This paper re-examines the hypothesis that tidal dissipation may destabilize Trojan exoplanets and prevent their long-term survival. The Appendix derives a theory of tidal forces generalized for systems with more than two bodies. Section 2 of the main text generalizes the CR3BP to include tidal forces on the third body, while Section 3 linearizes the equations of motion for small departures from L4 or L5. Section 4 analytically solves the linearized equation of vertical motion, while Section 5 solves the linearized equations of horizontal motion analytically. For comparison, Section 6 displays particular numerical solutions of the non-linearized equations; some readers may wish to skip directly to this section. Finally, Section 7 discusses our conclusions.

2 Model

For this study, we envision a primary of stellar mass M_1 (a star or a compact object) orbited by a secondary of sub-stellar mass $M_2 < M_1$ (a giant planet or a brown dwarf), and also by a third body of small mass $m_o \ll M_2$ (a terrestrial planet or a super-Earth), so that it does not significantly affect the motions of M_1 or M_2 . All three objects are assumed to be essentially spherical, and the secondary M_2 is assumed to be in a fixed orbit of semi-major axis σ and negligible eccentricity about the primary M_1 ; while the tertiary body m_o is assumed already to be despun to synchronous rotation by tides, and librating about the secondary's Trojan point L4 or L5. Then the question is whether this libration is damped or pumped by the action of tides in the tertiary. Note that we neglect tides in the primary and secondary, because tidal dissipation in stars and giant planets is normally weak compared to that in solid/liquid bodies such as terrestrial planets (but see Lainey *et al*, 2020).

We apply the machinery of the Circular Restricted Three-Body Problem (CR3BP) to the above model; symbols are defined in Tables 1 and 2. As usual, we define a synodic Cartesian coordinate system X, Y, Z (with corresponding unit vectors $\mathbf{I}, \mathbf{J}, \mathbf{K}$) where both M_1 and M_2 are fixed, with its origin at their mutual center of mass. Let this system rotate counter-clockwise about its $+Z$ axis with angular velocity equal to that of M_2 about M_1 , of magnitude $n = \sqrt{G[M_1 + M_2]}/\sigma^3$, where G is Newton's constant of universal gravitation. For convenience, we choose units of time, length, and mass such that n, σ , and $[M_1 + M_2]$ all equal one; then G also becomes unity.

Furthermore, let the X axis of these coordinates pass through both M_1 and M_2 , so that the primary is fixed at point $(X, Y, Z) = (-M_2, 0, 0)$, while the secondary resides at point $(M_1, 0, 0)$. Finally, the Y axis completes a right-handed triad. Then the leading equilateral point L4 lies at $(1/2 - M_2, +\sqrt{3}/4, 0)$ while the trailing equilateral point L5 lies at $(1/2 - M_2, -\sqrt{3}/4, 0)$.

In this synodic frame of reference, the equations of motion for a particle of negligible mass m_o become

$$\ddot{X} = 2\dot{Y} + X + f_X + \partial U / \partial X, \quad (1)$$

$$\ddot{Y} = -2\dot{X} + Y + f_Y + \partial U / \partial Y, \quad (2)$$

$$\text{and } \ddot{Z} = f_Z + \partial U / \partial Z. \quad (3)$$

Here f_X, f_Y , and f_Z are the components of \mathbf{f} , the acceleration of m_o due to tides, in the $+X, +Y$, and $+Z$ directions, respectively; formulae for the corresponding tidal forces $\mathbf{F} = m_o \mathbf{f}$ are developed in the Appendix.

In System (1) through (3) above, U is just minus the usual gravitational potential:

$$U = M_1/r_1 + M_2/r_2. \quad (4)$$

Here r_1 and r_2 are the distances of m_o from the centers of M_1 and M_2 respectively, given by

$$r_1 = \sqrt{(X + M_2)^2 + Y^2 + Z^2} \quad \text{and} \quad r_2 = \sqrt{(X - M_1)^2 + Y^2 + Z^2}; \quad (5)$$

note that U is always positive. Then differentiating Formula (4) gives

$$\partial U / \partial X = -M_1[X + M_2]r_1^{-3} - M_2[X - M_1]r_2^{-3}, \quad (6)$$

$$\partial U / \partial Y = -M_1 Y r_1^{-3} - M_2 Y r_2^{-3}, \quad (7)$$

$$\partial U / \partial Z = -M_1 Z r_1^{-3} - M_2 Z r_2^{-3}. \quad (8)$$

Table 1. Roman Symbols.

A_N	real part of α_N
a_n	imaginary part of α_N
B_N	real part of β_N
b_n	imaginary part of β_N
C_J	Jacobi constant
C	cosine coefficient of free vertical motion
c	cosine coefficient of forced vertical motion
D, E	complex amplitudes of free horizontal motion
e	orbital eccentricity
\mathbf{F}	$= m_o \mathbf{f}$ = tidal force on m_o
\mathbf{f}	tidal acceleration of m_o
G	Newton's constant of universal gravitation
g	surface gravity on m_o
H	complex amplitude of free vertical motion
h	second-degree height Love number
i	orbital inclination from the XY plane
j	imaginary unit; $j^2 = -1$
k	second-degree potential Love number
$\mathbf{I}, \mathbf{J}, \mathbf{K}$	unit vectors in directions of increasing X, Y, Z
$L4$	leading equilateral Lagrange point
$L'4$	tidally shifted location of $L4$
$L5$	trailing equilateral Lagrange point
$L'5$	tidally shifted location of $L5$
ℓ_N	angular frequencies of horizontal motion
M	mass of tide-raising body
M_1	mass of primary
M_2	mass of secondary ($< M_1$)
m	mass of perturbed body
m_o	mass of tertiary ($<< M_2$)
N	integer index
n	mean motion = $\sqrt{G[M_1 + M_2]}/a_2^3$
P	period of tides
Q	tidal quality factor
q_N	complex quotient β_N/α_N
R	radius of m_o
R_1	radius of M_1
\mathbf{r}	current location of tide-raising body relative to m_o
\mathbf{r}'	time-lagged location of tide-raising body relative to m_o
r_o	distance from center of m_o
r_1	distance between m_o and M_1
r_2	distance between m_o and M_2
S	sine coefficient of free vertical motion
s	sine coefficient of forced vertical motion
t	time
U	(minus) gravitational potential
V_1	tidal potential from M_1
V_2	tidal potential from M_2
V'	lagged tidal potential
W_1	quadrupole potential raised by M_1
W_2	quadrupole potential raised by M_2
X, Y, Z	global Cartesian coordinates
x, y, z	local Cartesian coordinates
x_0, y_0, z_0	initial values of $x - x', y - y'$, and z , respectively
x', y'	horizontal offsets of equilibria from $L4$ or $L5$

Table 2. Greek Symbols.

α_N	complex coefficients in Formula (75)
β_N	complex coefficients in Formula (76)
Γ	defined by Formula (74)
γ_N	complex roots of biquadratic Eq. (55)
Δ	defined by Formula (73)
δ_N	$\lambda_N - \gamma_N$
ε	angle between \mathbf{K} and $\boldsymbol{\omega}$ in the sidereal frame
ζ	e-folding rate of free vertical motion
η	angular frequency of free vertical motion
θ_1	angular distance from sub- M_1 point on m_o
θ_2	angular distance from sub- M_2 point on m_o
Θ	angular distance between M_1 and M_2 at m_o
κ	tidal constant defined by Formula (26)
κ_c	critical value of κ
Λ_N	e-folding rates of horizontal motion
λ_N	complex rate constants of horizontal motion
ν	complex rate constant of free vertical motion
ρ	mean density of m_o
σ	orbital semi-major axis of M_2 about M_1
τ	tidal time lag
$\boldsymbol{\omega}$	spin angular velocity of m_o
$\boldsymbol{\omega}$	apparent transverse velocity $\mathbf{r} \times \boldsymbol{\omega}$

When dissipative tides are included, System (1) through (3) does not conserve energy, and does not possess any isolating integrals. However, if f is neglected, System (1) through (3) is conservative, and possesses a single isolating integral

$$C_J = 2U + X^2 + Y^2 - \dot{X}^2 - \dot{Y}^2 - \dot{Z}^2 + M_1 M_2 \quad (9)$$

called the Jacobi constant (also known as the Tisserand parameter), equal to -2 times the total energy per unit mass of μ (gravitational potential +centrifugal potential +specific kinetic energy). The arbitrary constant of integration has been set to $M_1 M_2$ by convention, so that $C_J = 3$ at L4 and L5 when $\dot{X} = \dot{Y} = \dot{Z} = 0$.

3 Linearization

In order to study the stability of small tadpole orbits, we linearize the equations of motion about the Trojan points. First, define local displacements (x, y, z) about these points, parallel to the global coordinates (X, Y, Z) ; but please note that this convention is *opposite* to that of Murray and Dermott (1999, p. 85). Then near the leading Trojan point L4,

$$X = x + 1/2 - M_2 = x + M_1 - 1/2, \quad Y = y + \sqrt{3/4}, \quad \text{and} \quad Z = z; \quad (10)$$

while near the trailing Trojan point L5,

$$X = x + 1/2 - M_2 = x + M_1 - 1/2, \quad Y = y - \sqrt{3/4}, \quad \text{and} \quad Z = z. \quad (11)$$

Note the sign difference in the Y coordinate; note also that $\dot{X} = \dot{x}$, $\ddot{X} = \ddot{x}$, *etc.*, and similarly for Y and Z .

In these local coordinates, System (1) through (3) becomes

$$\ddot{x} = 2\dot{y} + x + 1/2 - M_2 + f_x + \partial U / \partial x, \quad (12)$$

$$\ddot{y} = -2\dot{x} + y \pm \sqrt{3/4} + f_y + \partial U / \partial y, \quad (13)$$

$$\text{and} \quad \ddot{z} = f_z + \partial U / \partial z. \quad (14)$$

In Eq. (13), and until further notice, the upper sign applies at the leading Trojan point L4, while the lower sign applies at the trailing Trojan point L5.

3.1 Potential

In System (12) through (14) above,

$$\partial U/\partial x = \partial U/\partial X = -M_1[X + M_2]r_1^{-3} - M_2[X - M_1]r_2^{-3} = -M_1[x + 1/2]r_1^{-3} - M_2[x - 1/2]r_2^{-3}, \quad (15)$$

$$\partial U/\partial y = \partial U/\partial Y = -M_1Yr_1^{-3} - M_2Yr_2^{-3} = -M_1[y \pm \sqrt{3/4}]r_1^{-3} - M_2[y \pm \sqrt{3/4}]r_2^{-3}, \quad (16)$$

$$\text{and } \partial U/\partial z = \partial U/\partial Z = -M_1Zr_1^{-3} - M_2Zr_2^{-3} = -M_1zr_1^{-3} - M_2zr_2^{-3}. \quad (17)$$

Linearizing Formulae (15) through (17) above is relatively easy. From Eqs. (5),

$$r_1 = \sqrt{(x + 1/2)^2 + (y \pm \sqrt{3/4})^2 + z^2} \approx \sqrt{1 + x \pm y\sqrt{3}} \approx 1 + x/2 \pm y\sqrt{3/4}, \quad (18)$$

while

$$r_2 = \sqrt{(x - 1/2)^2 + (y \pm \sqrt{3/4})^2 + z^2} \approx \sqrt{1 - x \pm y\sqrt{3}} \approx 1 - x/2 \pm y\sqrt{3/4}, \quad (19)$$

to first degree in the local coordinates.

Substituting Formulae (18) and (19) above for r_1 and r_2 into Eqs. (15) through (17) gives

$$\partial U/\partial x = -M_1[x + 1/2]r_1^{-3} - M_2[x - 1/2]r_2^{-3} \quad (20)$$

$$\approx -M_1[x + 1/2][1 - 3x/2 \mp 3y\sqrt{3/4}] - M_2[x - 1/2][1 + 3x/2 \mp 3y\sqrt{3/4}]$$

$$\approx -M_1[1/2 + x/4 \mp 3\sqrt{3}y/4] - M_2[-1/2 + x/4 \pm 3\sqrt{3}y/4]$$

$$= -(M_1 - M_2)[1/2 \mp 3\sqrt{3}y/4] - (M_1 + M_2)x/4$$

$$= -(1 - 2M_2)[1/2 \mp 3\sqrt{3}y/4] - x/4,$$

$$\partial U/\partial y = -M_1[y \pm \sqrt{3/4}]r_1^{-3} - M_2[y \pm \sqrt{3/4}]r_2^{-3} \quad (21)$$

$$\approx -M_1[y \pm \sqrt{3/4}][1 - 3x/2 \mp 3y\sqrt{3/4}] - M_2[y \pm \sqrt{3/4}][1 + 3x/2 \mp 3y\sqrt{3/4}]$$

$$\approx -M_1[\pm\sqrt{3/4} \mp 3\sqrt{3}x/4 - 5y/4] - M_2[\pm\sqrt{3/4} \pm 3\sqrt{3}x/4 - 5y/4],$$

$$= -(M_1 + M_2)[\pm\sqrt{3/4} - 5y/4] \pm 3\sqrt{3}(M_1 - M_2)x/4$$

$$= \mp\sqrt{3/4} + 5y/4 \pm 3\sqrt{3}(1 - 2M_2)x/4,$$

$$\text{and } \partial U/\partial z = -M_1zr_1^{-3} - M_2zr_2^{-3} \approx -M_1z - M_2z = -(M_1 + M_2)z = -z, \quad (22)$$

again to first degree in the local coordinates.

Then substituting Formulae (20) through (22) above into System (12) through (14) and simplifying gives

$$\ddot{x} = +2\dot{y} + 3x/4 \pm 3\sqrt{3}(1 - 2M_2)y/4 + f_x, \quad (23)$$

$$\ddot{y} = -2\dot{x} + 9y/4 \pm 3\sqrt{3}(1 - 2M_2)x/4 + f_y, \quad (24)$$

$$\text{and } \ddot{z} = -z + f_z. \quad (25)$$

Note that Eqs. (23) and (24) reduce to Eqs. (3.101) and (3.140) of Murray & Dermott (1999) when the tidal terms are neglected.

3.2 Tidal terms

The Appendix gives vectorial formulae for the tidal forces \mathbf{F} on m_o , in dimensional units. Now we must express these as dimensionless accelerations \mathbf{f} , in Cartesian coordinates. To convert the tidal force \mathbf{F} into the corresponding acceleration \mathbf{f} , divide the force by the mass m_o of the tertiary body. This presents no difficulties even if m_o approaches zero, because each of the four force terms \mathbf{F}_{11} , \mathbf{F}_{12} , \mathbf{F}_{21} , and \mathbf{F}_{22} contains a factor of kR^5 , while its mass $m_o = 4\pi\rho R^3/3$ scales only as the cube of its radius (for a given mean density ρ). Then the net acceleration \mathbf{f} scales as kR^2 .

In order to render \mathbf{f} dimensionless in the context of the Three-Body Problem, we also must divide it by the constant $\sigma n^2 = G[M_1 + M_2]/\sigma^2$, with dimensions of acceleration. For convenience, we define the constant coefficient

$$\kappa \equiv \frac{3kGR^5}{m_o\sigma n^2} = \frac{3kGR^5}{4\pi\rho R^3\sigma n^2/3} = \frac{9kGR^2}{4\pi\rho\sigma n^2} = \frac{9kGR^2\sigma^2}{4\pi\rho G[M_1 + M_2]} = \frac{9kR^2\sigma^2}{4\pi\rho[M_1 + M_2]}, \quad (26)$$

with dimensions of Length⁷/Mass².

If m_o has a similar density to the primary M_1 , then κ is of order $R^2R_1^3/\sigma^5$ or less in dimensionless units, where R_1 is the radius of the primary. Thus for most astrophysical situations, κ is much less than unity. For the Earth-Moon system, for example, $R \approx 1738$ km, $R_1 \approx 6378$ km, and $\sigma \approx 384\,000$ km, so κ is on the order of 10^{-10} or less; while for the Sun-Earth system, $R \approx 6378$ km, $R_1 \approx 696\,000$ km, and $\sigma \approx 150 \times 10^6$ km, so $\kappa \ll 2 \times 10^{-16}$!

The formulae for \mathbf{F} in the Appendix already have been linearized in the tidal time lag τ , but now they must be linearized in the local coordinates x, y, z as well. Because M_1 and M_2 are fixed in the synodic frame, only the coordinates of m_o vary. Then the expressions of the Appendix can be written as in Table 3, to first degree in x, y , and z . Note from this table that \mathbf{r}_1 and \mathbf{r}_2 are equal; furthermore, $\mathbf{r}_1 \bullet \dot{\mathbf{r}}_2 \approx \dot{r}_1$ and $\mathbf{r}_2 \bullet \dot{\mathbf{r}}_1 \approx \dot{r}_2$. These result in some welcome simplifications to the formulae for \mathbf{F} and \mathbf{f} . An even greater simplification is also possible, as follows.

We define a planet's obliquity ε as the angle between its orbit normal \mathbf{K} and its rotational angular velocity $\boldsymbol{\omega}$, in the sidereal frame. Most planets and asteroids in our Solar System start with a wide range of obliquities, and rotation periods of about half a day to one day. However, planets massive enough and close enough to their parent star to be affected significantly by solar tides despin to low obliquities and slow rotations within the first 10^9 years (*e.g.*, Dobrovolskis, 2007).

In our own Solar System, Mercury has been captured into a spin-orbit resonance such that it rotates three times during every two orbits, because of its permanent quadrupole moment and its relatively high orbital eccentricity $e \approx 0.206$ (*e.g.*, Noyelles *et al.*, 2014); while Venus presumably has been caught in a balance between gravitational tides in its interior and thermal tides in its massive atmosphere (*e.g.*, Ingersoll and Dobrovolskis, 1978).

Most regular satellites of the Sun's planets are locked into synchronous rotation, so that their spin periods exactly match their orbit periods. Furthermore, their obliquities with respect to their orbits are small; thus they always keep nearly the same hemisphere facing toward their parent planets, as our Moon always presents roughly the same face to the Earth. This appears to be the most likely outcome for despun solid exoplanets with low orbital eccentricities, as well. Fluid exoplanets may despin to a "pseudo-synchronous" state with $\omega/n \approx (1 + 5e^2)/(1 - e^2)$ (Dobrovolskis, 2007; see also Hut, 1981).

Henceforth we assume synchronous rotation of m_o , with low obliquity ε . Then in the synodic frame where M_1 and M_2 both are fixed, the Z component of $\boldsymbol{\omega}$ vanishes to first degree in ε , leaving

$$\boldsymbol{\omega} = -\mathbf{I}\varepsilon \sin(t) - \mathbf{J}\varepsilon \cos(t). \quad (27)$$

Without loss of generality, here we have chosen the origin of time when $\boldsymbol{\omega}$ points in the $-Y$ direction; if m_o were in a Keplerian orbit lying in the XY plane, this would correspond to its northern vernal equinox.

Table 3. Linearized expressions.

Expression	Linearization
\mathbf{r}_1	$(-x - 1/2)\mathbf{I} + (-y \mp \sqrt{3}/4)\mathbf{J} - z\mathbf{K}$
\mathbf{r}_2	$(-x + 1/2)\mathbf{I} + (-y \mp \sqrt{3}/4)\mathbf{J} - z\mathbf{K}$
r_1^2	$1 + x \pm y\sqrt{3}$
r_2^2	$1 - x \pm y\sqrt{3}$
r_1	$1 + x/2 \pm y\sqrt{3}/4$
r_2	$1 - x/2 \pm y\sqrt{3}/4$
$r_1 r_2$	$1 \pm y\sqrt{3}$
\dot{r}_1	$+\dot{x}/2 \pm \dot{y}\sqrt{3}/4$
\dot{r}_2	$-\dot{x}/2 \pm \dot{y}\sqrt{3}/4$
$\dot{\mathbf{r}}_1$	$-\dot{x}\mathbf{I} - \dot{y}\mathbf{J} - \dot{z}\mathbf{K}$
$\dot{\mathbf{r}}_2$	$-\dot{x}\mathbf{I} - \dot{y}\mathbf{J} - \dot{z}\mathbf{K}$
$\mathbf{r}_1 \bullet \mathbf{r}_2$	$1/2 \pm y\sqrt{3}$
$\mathbf{r}_1 \bullet \dot{\mathbf{r}}_2$	$+\dot{x}/2 \pm \dot{y}\sqrt{3}/4$
$\mathbf{r}_2 \bullet \dot{\mathbf{r}}_1$	$-\dot{x}/2 \pm \dot{y}\sqrt{3}/4$
$\boldsymbol{\omega}_1 = \mathbf{r}_1 \times \boldsymbol{\omega}$	$(z\omega_y - y\omega_z \mp \sqrt{3}/4\omega_z)\mathbf{I}$ $-(z\omega_x - x\omega_z - \omega_z/2)\mathbf{J}$ $+(y\omega_x \pm \sqrt{3}/4\omega_x - x\omega_y - \omega_y/2)\mathbf{K}$
$\boldsymbol{\omega}_2 = \mathbf{r}_2 \times \boldsymbol{\omega}$	$(z\omega_y - y\omega_z \mp \sqrt{3}/4\omega_z)\mathbf{I}$ $-(z\omega_x - x\omega_z + \omega_z/2)\mathbf{J}$ $+(y\omega_x \pm \sqrt{3}/4\omega_x - x\omega_y + \omega_y/2)\mathbf{K}$

From Table 3 and Formula (27) above, the transverse velocities $\boldsymbol{\omega}_1$ and $\boldsymbol{\omega}_2$ then reduce to vertical velocities $\boldsymbol{\omega}_1\mathbf{K}$ and $\boldsymbol{\omega}_2\mathbf{K}$, respectively, where

$$\boldsymbol{\omega}_1 = \pm\sqrt{3/4}\omega_x - \omega_y/2 = \varepsilon[\mp\sqrt{3}\sin(t) + \cos(t)]/2 \quad (28)$$

and

$$\boldsymbol{\omega}_2 = \pm\sqrt{3/4}\omega_x + \omega_y/2 = \varepsilon[\mp\sqrt{3}\sin(t) - \cos(t)]/2, \quad (29)$$

to first degree in the small quantities x, y, z , and ε .

From Formulae (26) and (28), and Formula (104) of the Appendix, the primary tidal term $\mathbf{f}_{11} = \mathbf{F}_{11}/m_o$ can be expressed as

$$\begin{aligned} \mathbf{f}_{11} &\approx \kappa M_1^2 r_1^{-8} \{ [1 + 2\dot{r}_1 \tau / r_1] \mathbf{r}_1 + [\dot{\mathbf{r}}_1 + \boldsymbol{\omega}_1] \tau \} \\ &\approx \kappa M_1^2 [1 - 4x \mp 4y\sqrt{3}] \{ [1 + (\dot{x} \pm \dot{y}\sqrt{3})\tau] [-(x + 1/2)\mathbf{I} - (y \pm \sqrt{3}/4)\mathbf{J} - z\mathbf{K}] - (\dot{x}\mathbf{I} + \dot{y}\mathbf{J} + [\dot{z} - \boldsymbol{\omega}_1]\mathbf{K})\tau \} \\ &\approx \kappa M_1^2 \{ [-\frac{1}{2} + x \pm 2y\sqrt{3} - \frac{3}{2}\dot{x}\tau \mp \sqrt{\frac{3}{4}}\dot{y}\tau]\mathbf{I} + [\mp\sqrt{\frac{3}{4}} \pm 2x\sqrt{3} + 5y \mp \sqrt{\frac{3}{4}}\dot{x}\tau - \frac{5}{2}\dot{y}\tau]\mathbf{J} - [z + \dot{z}\tau - \boldsymbol{\omega}_1\tau]\mathbf{K} \}. \end{aligned} \quad (30)$$

Similarly, linearizing Formula (105) of the Appendix gives the secondary tidal term

$$\begin{aligned} \mathbf{f}_{22} &\approx \kappa M_2^2 r_2^{-8} \{ [1 + 2\dot{r}_2 \tau / r_2] \mathbf{r}_2 + [\dot{\mathbf{r}}_2 + \boldsymbol{\omega}_2] \tau \} \\ &\approx \kappa M_2^2 [1 + 4x \mp 4y\sqrt{3}] \{ [1 + (-\dot{x} \pm \dot{y}\sqrt{3})\tau] [-(x - 1/2)\mathbf{I} - (y \pm \sqrt{3}/4)\mathbf{J} - z\mathbf{K}] - (\dot{x}\mathbf{I} + \dot{y}\mathbf{J} + [\dot{z} - \boldsymbol{\omega}_2]\mathbf{K})\tau \} \\ &\approx \kappa M_2^2 \{ [+ \frac{1}{2} + x \mp 2y\sqrt{3} - \frac{3}{2}\dot{x}\tau \pm \sqrt{\frac{3}{4}}\dot{y}\tau]\mathbf{I} + [\mp\sqrt{\frac{3}{4}} \mp 2x\sqrt{3} + 5y \pm \sqrt{\frac{3}{4}}\dot{x}\tau - \frac{5}{2}\dot{y}\tau]\mathbf{J} - [z + \dot{z}\tau - \boldsymbol{\omega}_2\tau]\mathbf{K} \}. \end{aligned} \quad (31)$$

Note the pattern of sign differences between Formulae (30) and (31) above.

Linearizing Formula (106) of the Appendix gives the first mixed term:

$$\begin{aligned}
\mathbf{f}_{12} &\approx \kappa M_1 M_2 r_1^{-5} r_2^{-7} \{ [5(\mathbf{r}_2 \bullet \mathbf{r}_1)^2 - 10(\mathbf{r}_2 \bullet \mathbf{r}_1)[\mathbf{r}_2 \bullet (\dot{\mathbf{r}}_1 + \boldsymbol{\omega}_1)]\tau - r_1^2 r_2^2 - 3r_2^2 r_1 \dot{r}_1 \tau] \mathbf{r}_2 / 2 \\
&\quad - [\mathbf{r}_2 \bullet (\mathbf{r}_1 - [\dot{\mathbf{r}}_1 + \boldsymbol{\omega}_1]\tau)] r_2^2 \mathbf{r}_1 + [\mathbf{r}_2 \bullet \mathbf{r}_1] r_2^2 (\dot{\mathbf{r}}_1 + \boldsymbol{\omega}_1)\tau + 5[5(\mathbf{r}_2 \bullet \mathbf{r}_1)^2 \mathbf{r}_2 / 2 - (\mathbf{r}_2 \bullet \mathbf{r}_1) r_2^2 \mathbf{r}_1] \dot{r}_1 \tau / r_1 \} \\
&\approx \kappa M_1 M_2 [1 - 5x/2 \mp 5y\sqrt{3/4}] [1 + 7x/2 \mp 7y\sqrt{3/4}] \{ [5(1/2 \pm y\sqrt{3})^2 - 10(1/2 \pm y\sqrt{3})(-\dot{x}/2 \pm \dot{y}\sqrt{3/4} - z\boldsymbol{\omega}_1)\tau \\
&\quad - (1 + x \pm y\sqrt{3})(1 - x \pm y\sqrt{3}) - 3(1 - x \pm y\sqrt{3})(1 + x/2 \pm y\sqrt{3/4})(+\dot{x}/2 \pm \dot{y}\sqrt{3/4})\tau] [(-x + 1/2)\mathbf{I} - (y \pm \sqrt{3/4})\mathbf{J} - z\mathbf{K}] / 2 \\
&\quad - [(1/2 \pm y\sqrt{3}) - (-\dot{x}/2 \pm \dot{y}\sqrt{3/4} - z\boldsymbol{\omega}_1)\tau] (1 - x \pm y\sqrt{3}) [(-x - 1/2)\mathbf{I} - (y \pm \sqrt{3/4})\mathbf{J} - z\mathbf{K}] \\
&\quad + [1/2 \pm y\sqrt{3}] (1 - x \pm y\sqrt{3}) [-\dot{x}\mathbf{I} - \dot{y}\mathbf{J} + (\boldsymbol{\omega}_1 - \dot{z})\mathbf{K}]\tau \\
&\quad + 5[5(1/2 \pm y\sqrt{3})^2 ((-x + 1/2)\mathbf{I} - (y \pm \sqrt{3/4})\mathbf{J} - z\mathbf{K}) / 2 - (1/2 \pm y\sqrt{3})(1 - x \pm y\sqrt{3}) ((-x - 1/2)\mathbf{I} - (y \pm \sqrt{3/4})\mathbf{J} - z\mathbf{K})] \\
&\quad \quad (1 - x/2 \mp y\sqrt{3/4})(\dot{x}/2 \pm \dot{y}\sqrt{3/4})\tau \} \\
&\approx \kappa M_1 M_2 \{ \mathbf{I} [\frac{5}{16} + \frac{7}{16}x + \frac{45}{32}\dot{x}\tau \mp \frac{3\sqrt{3}}{8}y \pm \frac{5\sqrt{3}}{32}\dot{y}\tau] \\
&\quad + \mathbf{J} [\pm \frac{3\sqrt{3}}{16} \mp \frac{\sqrt{3}}{16}x \mp \frac{5\sqrt{3}}{32}\dot{x}\tau - 3y + \frac{41}{32}\dot{y}\tau] + \mathbf{K} [\frac{3}{8}z + \frac{1}{2}(\boldsymbol{\omega}_1 - \dot{z})\tau] \}. \tag{32}
\end{aligned}$$

Then swapping subscripts in Formula (32) above gives the second mixed term:

$$\begin{aligned}
\mathbf{f}_{21} &\approx \kappa M_1 M_2 r_2^{-5} r_1^{-7} \{ [5(\mathbf{r}_1 \bullet \mathbf{r}_2)^2 - 10(\mathbf{r}_1 \bullet \mathbf{r}_2)[\mathbf{r}_1 \bullet (\dot{\mathbf{r}}_2 + \boldsymbol{\omega}_2)]\tau - r_1^2 r_2^2 - 3r_1^2 r_2 \dot{r}_2 \tau] \mathbf{r}_1 / 2 \\
&\quad - [\mathbf{r}_1 \bullet (\mathbf{r}_2 - [\dot{\mathbf{r}}_2 + \boldsymbol{\omega}_2]\tau)] r_1^2 \mathbf{r}_2 + [\mathbf{r}_1 \bullet \mathbf{r}_2] r_1^2 (\dot{\mathbf{r}}_2 + \boldsymbol{\omega}_2)\tau + 5[5(\mathbf{r}_1 \bullet \mathbf{r}_2)^2 \mathbf{r}_1 / 2 - (\mathbf{r}_1 \bullet \mathbf{r}_2) r_1^2 \mathbf{r}_2] \dot{r}_2 \tau / r_2 \} \\
&\approx \kappa M_1 M_2 (1 + 5x/2 \mp 5y\sqrt{3/4})(1 - 7x/2 \mp 7y\sqrt{3/4}) \{ [5(1/2 \pm y\sqrt{3})^2 - 10(1/2 \pm y\sqrt{3})(+\dot{x}/2 \pm \dot{y}\sqrt{3/4} - z\boldsymbol{\omega}_2)\tau \\
&\quad - (1 \pm y\sqrt{3})^2 - 3(1 \pm y\sqrt{3})(1 + x/2 \pm y\sqrt{3/4})(-\dot{x}/2 \pm \dot{y}\sqrt{3/4})\tau] [(-x - 1/2)\mathbf{I} - (y \pm \sqrt{3/4})\mathbf{J} - z\mathbf{K}] / 2 \\
&\quad - [(1/2 \pm y\sqrt{3}) - (+\dot{x}/2 \pm \dot{y}\sqrt{3/4} - z\boldsymbol{\omega}_2)\tau] (1 + x \pm y\sqrt{3}) [(-x + 1/2)\mathbf{I} - (y \pm \sqrt{3/4})\mathbf{J} - z\mathbf{K}] \\
&\quad + [1/2 \pm y\sqrt{3}] (1 + x \pm y\sqrt{3}) [-\dot{x}\mathbf{I} - \dot{y}\mathbf{J} + (\boldsymbol{\omega}_2 - \dot{z})\mathbf{K}]\tau \\
&\quad + 5[5(1/2 \pm y\sqrt{3})^2 ((-x - 1/2)\mathbf{I} - (y \pm \sqrt{3/4})\mathbf{J} - z\mathbf{K}) / 2 - (1/2 \pm y\sqrt{3})(1 + x \pm y\sqrt{3}) ((-x + 1/2)\mathbf{I} - (y \pm \sqrt{3/4})\mathbf{J} - z\mathbf{K})] \\
&\quad \quad (1 + x/2 \mp y\sqrt{3/4})(-\dot{x}/2 \pm \dot{y}\sqrt{3/4})\tau \} \\
&\approx \kappa M_1 M_2 \{ \mathbf{I} [-\frac{5}{16} + \frac{7}{16}x + \frac{45}{32}\dot{x}\tau \pm \frac{3\sqrt{3}}{8}y \mp \frac{5\sqrt{3}}{32}\dot{y}\tau] \\
&\quad + \mathbf{J} [\pm \frac{3\sqrt{3}}{16} \pm \frac{\sqrt{3}}{16}x \pm \frac{5\sqrt{3}}{32}\dot{x}\tau - 3y + \frac{41}{32}\dot{y}\tau] + \mathbf{K} [\frac{3}{8}z + \frac{1}{2}(\boldsymbol{\omega}_2 - \dot{z})\tau] \}. \tag{33}
\end{aligned}$$

Note the pattern of sign differences between Formulae (32) and (33) above, like that between Formulae (30) and (31). This leads to substantial simplifications when Formulae (32) and (33) are added together into a joint mixed term:

$$\mathbf{f}_{12} + \mathbf{f}_{21} \approx \kappa M_1 M_2 \{ \mathbf{I} [\frac{7}{8}x + \frac{45}{16}\dot{x}\tau] + \mathbf{J} [\pm \frac{3\sqrt{3}}{8} - 6y + \frac{41}{16}\dot{y}\tau] + \mathbf{K} [\frac{3}{4}z + \frac{1}{2}(\boldsymbol{\omega}_1 + \boldsymbol{\omega}_2)\tau - \dot{z}\tau] \}. \tag{34}$$

Note also that $(\varpi_1 + \varpi_2)$ reduces to just $\pm\sqrt{3}\omega_x = \mp\varepsilon\sqrt{3}\sin t$ from Formulae (28) and (29).

Finally, Formulae (30), (31), and (34) above all can be combined to give the net tidal accelerations for System (23) through (25):

$$\begin{aligned}
f_x &= \kappa[(M_2^2 - M_1^2)/2 + (M_1^2 + M_2^2 + 7M_1M_2/8)x + (45M_1M_2/16 - 3M_1^2/2 - 3M_2^2/2)\dot{x}\tau \\
&\quad \pm 2\sqrt{3}(M_1^2 - M_2^2)y \pm \sqrt{3}(M_2^2 - M_1^2)\dot{y}\tau/2] \\
&= \kappa[(M_2 - M_1)/2 + (1 - 9M_1M_2/8)x + (93M_1M_2/16 - 3/2)\dot{x}\tau \\
&\quad \pm \sqrt{3}(M_1 - M_2)(2y - \dot{y}\tau/2)], \tag{35}
\end{aligned}$$

$$\begin{aligned}
f_y &= \kappa[\pm\sqrt{3}(3M_1M_2/8 - M_1^2/2 - M_2^2/2) \pm 2\sqrt{3}(M_1^2 - M_2^2)x \mp \sqrt{3}(M_1^2 - M_2^2)\dot{x}\tau/2 \\
&\quad + (5M_1^2 + 5M_2^2 - 6M_1M_2)y + (41M_1M_2/16 - 5M_1^2/2 - 5M_2^2/2)\dot{y}\tau] \\
&= \kappa[\pm\sqrt{3}(11M_1M_2/8 - 1/2) \pm \sqrt{3}(M_1 - M_2)(2x - \dot{x}\tau/2) \\
&\quad + (5 - 16M_1M_2)y + (121M_1M_2/16 - 5/2)\dot{y}\tau], \tag{36}
\end{aligned}$$

$$\begin{aligned}
f_z &= -\kappa[(M_1^2 + M_2^2 - 3M_1M_2/4)z + (M_1^2 + M_2^2 + M_1M_2)\dot{z}\tau + (M_1^2s_1 + M_2^2s_2 + M_1M_2(s_1 + s_2)/2)\tau] \\
&= -\kappa[(1 - 11M_1M_2/4)z + (1 - M_1M_2)\tau\dot{z} + (M_1^2\varpi_1 + M_2^2\varpi_2 + M_1M_2[\varpi_1 + \varpi_2]/2)\tau]. \tag{37}
\end{aligned}$$

Here we have used $M_1 + M_2 = 1$ to simplify Formulae (35) through (37) above slightly.

4 Vertical Motion

Substituting Formulae (35) through (37) into Eqs. (23) through (25), respectively, leaves Eqs. (23) and (24) a coupled system in x , y , and their derivatives; but Eq. (25) in z , \dot{z} , and \ddot{z} remains decoupled from System (23) and (24). Therefore we begin by solving Eq. (25) for the vertical motion of m_o .

Substituting Formulae (28), (29), and (37) into Eq. (25) gives

$$\begin{aligned}
\ddot{z} - \kappa\tau[1 - M_1M_2]\dot{z} + (1 + \kappa[1 - 11M_1M_2/4])z &= -\kappa\tau[M_1^2\varpi_1 + M_2^2\varpi_2 + M_1M_2[\varpi_1 + \varpi_2]/2] \\
&= -\kappa\tau\varepsilon[\mp\sqrt{3}(M_1^2 + M_2^2 + 2M_1M_2)\sin(t) + (M_1^2 - M_2^2)\cos(t)]/2 \\
&= -\kappa\tau\varepsilon[\mp\sqrt{3}\sin(t) + (M_1 - M_2)\cos(t)]/2, \tag{38}
\end{aligned}$$

with the homogeneous part on the left-hand side, and the forcing terms on the right.

4.1 Forced solution

The general solution to Eq. (38) above consists of a free part and a forced part. Because the forcing terms are sinusoidal, the forced solution is also sinusoidal, of the form $z_{forced} = s\sin(t) + c\cos(t)$, where the coefficients s and c are real constants. Substituting this into Eq. (38) gives

$$\begin{aligned}
-s\sin(t) - c\cos(t) - \kappa\tau[1 - M_1M_2][s\cos(t) - c\sin(t)] + (1 + \kappa[1 - 11M_1M_2/4])[s\sin(t) + c\cos(t)] \\
= -\kappa\tau\varepsilon[\mp\sqrt{3}\sin(t) + (M_1 - M_2)\cos(t)]/2. \tag{39}
\end{aligned}$$

Then equating sine terms gives

$$\kappa[1 - 11M_1M_2/4]s + \kappa\tau[1 - M_1M_2]c = \pm\kappa\tau\varepsilon\sqrt{3/4}, \tag{40}$$

while equating cosine terms gives

$$-\kappa\tau[1 - M_1M_2]s + \kappa[1 - 11M_1M_2/4]c = -\kappa\tau\varepsilon[M_1 - M_2]/2. \quad (41)$$

Simultaneously solving Eqs. (40) and (41) above gives

$$s \approx \frac{\pm 2\sqrt{3}\tau\varepsilon}{4 - 11M_1M_2} \quad \text{and} \quad c \approx \frac{-2\tau\varepsilon[M_1 - M_2]}{4 - 11M_1M_2}. \quad (42)$$

Here we have neglected terms of order τ^2 and higher, for consistency with the development of the Appendix. Solution (42) above represents m_o moving in a certain “preferred” orbital plane, tilted from the XY plane by an inclination angle

$$i = \sqrt{s^2 + c^2} = \frac{2\tau\varepsilon}{4 - 11M_1M_2} \sqrt{3 + [M_1 - M_2]^2} = \frac{4\tau\varepsilon\sqrt{1 - M_1M_2}}{4 - 11M_1M_2}. \quad (43)$$

Note that Formulae (42) and (43) above are independent of κ , as long as $\kappa \neq 0$; however, when $\kappa = 0$, the tides vanish, s , c , and i are arbitrary, and there is no preferred plane.

Figure 1 graphs $|s|$, $|c|$, and i as functions of M_2 (or of M_1) from Formulae (42) and (43), for M_2 up to $1/2$, for completeness. In the two-body case when $M_1 = 1$, so M_2 vanishes (left-hand axis), then $s = \pm\tau\varepsilon\sqrt{3}/4 \approx \pm 0.866\,025\,\tau\varepsilon$, $c = -\tau\varepsilon/2$, and $i = \tau\varepsilon$. When $M_1 = 1/2 + \sqrt{5/44} \approx 0.837\,100$ and $M_2 = 1/2 - \sqrt{5/44} \approx 0.162\,900$, c reaches a shallow minimum of $-4\tau\varepsilon/\sqrt{55} \approx -0.539\,360\,\tau\varepsilon$, while $s = \pm 4\sqrt{3}\tau\varepsilon/5 \approx \pm 1.385\,641\,\tau\varepsilon$ and $i = 8\sqrt{19/22}\,\tau\varepsilon/5 \approx 1.486\,913\,\tau\varepsilon$. However, in the “Copenhagen” case when $M_1 = M_2 = 1/2$ (right-hand edge), $|s|$ and i both peak at $8\sqrt{3}\tau\varepsilon/5 \approx 2.771\,281\,\tau\varepsilon$, while c vanishes entirely.

4.2 Free solution

For the free solution, we assume the form $z = H \exp(\nu t)$, where H is a complex amplitude of vertical motion and ν is its complex rate constant. Then substituting this into Eq. (25) gives the quadratic equation

$$\nu^2 = -1 - \kappa[1 - 11M_1M_2/4] - \kappa[1 - M_1M_2]\nu\tau, \quad (44)$$

with the two roots

$$\begin{aligned} \nu &= -\kappa\tau[1 - M_1M_2]/2 \pm \sqrt{\kappa^2\tau^2[1 - M_1M_2]^2/4 - 1 - \kappa[1 - 11M_1M_2/4]} \\ &\approx -\kappa\tau[1 - M_1M_2]/2 \pm \sqrt{-1 - \kappa[1 - 11M_1M_2/4]} \end{aligned} \quad (45)$$

to first degree in τ , where for the moment \pm has its usual meaning.

Note that the discriminant $-1 - \kappa[1 - 11M_1M_2/4]$ in Formula (45) above is always negative, because $[1 - 11M_1M_2/4]$ is always positive. Therefore ν can be written as $\zeta \pm j\eta$, where $\zeta = -\kappa\tau[1 - M_1M_2]/2$ is the e-folding rate of the free solution, $\eta = \sqrt{1 + \kappa[1 - 11M_1M_2/4]}$ is the angular frequency of its oscillations, and j is the imaginary unit ($j^2 = -1$). In strictly real terms, the complete free solution to Eq. (38) can be written as

$$z_{free} = \exp(\zeta t)[S \sin(\eta t) + C \cos(\eta t)], \quad (46)$$

where S and C are real constants. Because ζ is always negative, the vertical motion is always stable.

It is of interest to consider special cases of Formula (46) above. When κ vanishes, Formula (45) reduces to just $\nu = +j$ or $\nu = -j$; so $\zeta = 0$ and $\eta = 1$, and Formula (46) becomes $z_{free} = S \sin(t) + C \cos(t)$. Then the Trojan executes harmonic oscillations above and below the plane $z = 0$ with angular frequency unity (or n , in dimensional units), as expected; and their absolute amplitude $|H| = \sqrt{S^2 + C^2}$ effectively becomes the inclination of the Trojan orbit to the XY plane.

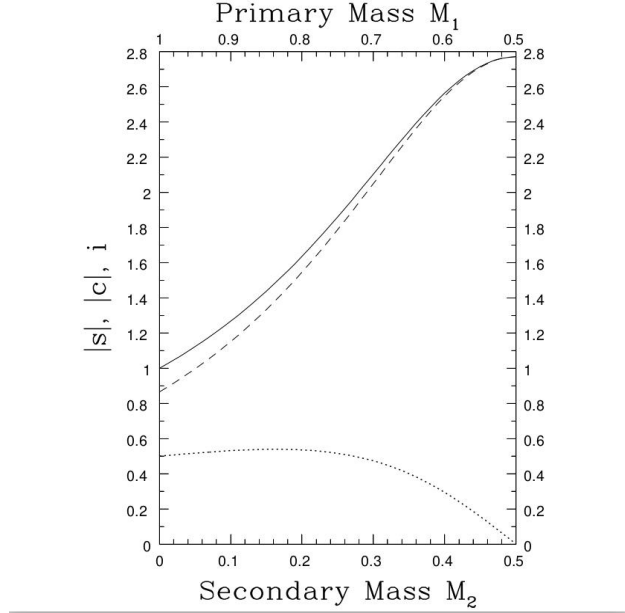


Figure 1: $|s|$ (dashed curve), $|c|$ (dotted curve), and i (solid curve), each normalized by $\tau\epsilon$, as functions of M_1 or of M_2 .

When the time lag τ vanishes, but κ does not, the Trojan still oscillates vertically about its preferred plane, again with effective inclination $|H| = \sqrt{S^2 + C^2}$, but now with slightly increased angular frequency $\eta = \sqrt{1 + \kappa[1 - 11M_1M_2/4]} \approx 1 + \kappa[1/2 - 11M_1M_2/8]$ due to the enhanced attraction of M_1 and M_2 on the tidal bulges of m_o .

When neither κ nor τ vanishes, the Trojan executes *damped* harmonic oscillations above and below the preferred plane, with essentially the same angular frequency η as above, but decaying to the preferred plane with e-folding time $-1/\zeta$ (or $-1/(2\pi\zeta)$ in orbital periods).

4.3 Complete solution

In order to evaluate the coefficients of the free solution (46), first write out the general solution to Eq. (38):

$$z = z_{forced} + z_{free} = s \sin(t) + c \cos(t) + \exp(-\zeta t)[S \sin(\eta t) + C \cos(\eta t)], \quad (47)$$

where s and c are given by Formulae (42). Then differentiating solution (47) above gives

$$\dot{z} = s \cos(t) - c \sin(t) + \exp(-\zeta t)[(S\eta - C\zeta) \cos(\eta t) - (C\eta + S\zeta) \sin(\eta t)]. \quad (48)$$

Next, set Formulae (47) and (48) above equal to their respective initial conditions $z = z_0$ and $\dot{z} = \dot{z}_0$ at time $t = 0$. Then solving the resulting two simultaneous equations gives

$$C = z_0 - c \text{ and } S = (\dot{z}_0 - s + C\zeta)/\eta. \quad (49)$$

In the dissipationless case when τ vanishes, then s , c , and ζ all vanish as well from Formulae (42) and (45); while Formulae (49) above reduce to $C = z_0$ and $S = \dot{z}_0$, and the general solution to Eq. (38) becomes just $z = \dot{z}_0 \sin(\eta t) + z_0 \cos(\eta t)$.

However, all of the above solutions are unrealistic, because they were obtained assuming that $\boldsymbol{\omega}$ was fixed in the sidereal frame. In reality, the equator plane of m_o would move, and would damp to its orbital plane much faster than *vice versa*, because the spin angular momentum of m_o is much less than its orbital angular momentum. Nevertheless, we conclude that the vertical motion of m_o is stable, and henceforth we confine ourselves to its horizontal motion.

5 Horizontal motion

The two-dimensional solution for the horizontal motion is generally more complicated than the one-dimensional solution for the vertical motion, because the x and y components are strongly coupled. Like the vertical solution, the horizontal solution consists of a free part and a forced part, but the forced part of the horizontal solution is constant rather than sinusoidal in time.

5.1 Shifted equilibria

To solve for the forced part of the horizontal motion, we assume that $x = x'$ and $y = y'$, where x' and y' are constants. Then Eqs. (23) and (24) respectively reduce to

$$\begin{aligned} 0 &= 3x'/4 \pm 3\sqrt{3}(1-2M_2)y'/4 + \kappa[(M_2-M_1)/2 + (1-9M_1M_2/8)x' \pm 2\sqrt{3}(M_1-M_2)y'] \\ &\approx 3x'/4 \pm 3\sqrt{3}[M_1-M_2]y'/4 - \kappa[M_1-M_2]/2 \end{aligned} \quad (50)$$

and

$$\begin{aligned} 0 &= 9y'/4 \pm 3\sqrt{3}(1-2M_2)x'/4 + \kappa[\pm\sqrt{3}(-1/2 + 11M_1M_2/8) \pm 2\sqrt{3}(M_1-M_2)x' + (5-16M_1M_2)y'] \\ &\approx 9y'/4 \pm 3\sqrt{3}[M_1-M_2]x'/4 \mp \kappa\sqrt{3}[1/2 - 11M_1M_2/8], \end{aligned} \quad (51)$$

where we neglect terms of order κ^2 and higher powers of κ .

Solving System (50) and (51) above gives

$$x' \approx 11\kappa[M_1-M_2]/24 \approx 0.458\,333\,\kappa[M_1-M_2] \quad (52)$$

and

$$y' \approx \pm 5\sqrt{3}\kappa/72 \approx \pm 0.120\,281\,\kappa, \quad (53)$$

provided that M_1M_2 does not vanish. Formulae (52) and (53) above represent a constant shift of the equilibrium points from the equilateral points L4 and L5 in the CR3BP without tides to the new equilibria L'4 and L'5, respectively, due to the enhanced attraction of M_1 and M_2 on the tidal bulges of m_o .

Note that x' vanishes when $M_1 = M_2$, and is positive when $M_1 > M_2$. The shift in y from the leading L4 point is non-negative, while that from the trailing L5 point is non-positive. Thus these equilibrium points lie farther from the origin with increasing κ , to compensate for the increased attraction of the tides. Note also that x' and y' both vanish when κ vanishes (provided that $M_2 \neq 0$), consistent with the classic CR3BP.

When M_2 vanishes, Eqs. (50) and (51) both reduce to $0 = x' \pm \sqrt{3}y' - 2\kappa/3$. This means that the equilibrium points may lie anywhere along a pair of infinitesimal arcs through L'4 and L'5 at a distance of $1 + \kappa/3$ from M_1 . This is consistent with the two-body problem including tides, and thus provides another valuable check on our results. Note that solutions (52) and (53) lie on these arcs. When κ vanishes as well, these arcs run through L4 and L5.

5.2 Characteristic equation

To find the free part of the solution to System (23) and (24), we assume solutions of the form $x = D \exp(\lambda t)$ and $y = E \exp(\lambda t)$, where D and E are complex amplitudes and λ is their shared complex rate constant. Then substituting these into Eqs. (23) and (24) gives

$$\lambda^2 D = 2\lambda E + 3D/4 \pm 3\sqrt{3}[M_1 - M_2]E/4 \quad (54)$$

$$+ \kappa[(1 - 9M_1M_2/8)D + (-3/2 + 93M_1M_2/16)D\lambda\tau \pm 2\sqrt{3}(M_1 - M_2)E \mp \sqrt{3}(M_1 - M_2)E\lambda\tau/2]$$

and

$$\lambda^2 E = -2\lambda D + 9E/4 \pm 3\sqrt{3}(M_1 - M_2)D/4 \quad (55)$$

$$+ \kappa[\pm 2\sqrt{3}(M_1 - M_2)D \mp \sqrt{3}(M_1 - M_2)D\lambda\tau/2 + (5 - 16M_1M_2)E + (-5/2 + 121M_1M_2/16)E\lambda\tau].$$

System (54) and (55) above consists of two homogeneous linear equations in the two unknowns, D and E . In matrix form, this system can be written as

$$\begin{bmatrix} 3/4 - \lambda^2 + \kappa[(1 - 9M_1M_2/8) - (3/2 - 93M_1M_2/16)\lambda\tau] & +2\lambda \pm 3\sqrt{3}(M_1 - M_2)/4 \pm \kappa\sqrt{3}(M_1 - M_2)[2 - \lambda\tau/2] \\ -2\lambda \pm 3\sqrt{3}(M_1 - M_2)/4 \pm \kappa\sqrt{3}(M_1 - M_2)[2 - \lambda\tau/2] & 9/4 - \lambda^2 + \kappa[(5 - 16M_1M_2) - (5/2 - 121M_1M_2/16)\lambda\tau] \end{bmatrix} \cdot \begin{bmatrix} D \\ E \end{bmatrix} = \begin{bmatrix} 0 \\ 0 \end{bmatrix}. \quad (56)$$

System (56) above is self-consistent only if the determinant of the coefficient matrix vanishes. To first degree in κ , this yields

$$0 = \lambda^4 + \lambda^2 + 27M_1M_2/4 + \kappa\lambda^3\tau[4 - 107M_1M_2/8] + \kappa\lambda^2[-6 + 137M_1M_2/8] + \kappa\lambda\tau[-3 + 39M_1M_2/4] + \kappa[-3 + 687M_1M_2/32]. \quad (57)$$

Eq. (57) above can be solved easily as a linear equation for M_1M_2 (or as a quadratic equation for M_2) as a function of κ and λ ; for example, $M_2 \approx M_1M_2 \approx 4\kappa/9$ when $\lambda = 0$. However, we wish to find λ as a function of M_2 and κ ; then Eq. (57) is a quartic equation, analytically solvable in principle, but cumbersome in practice. Its four roots λ_N may be real or complex (where the index N runs from 1 through 4); but any complex roots must come in conjugate pairs, because all of the coefficients in Eq. (57) are real.

5.3 Perturbation method

Consistent with our neglect of κ^2 , we approximate the roots of Eq. (57) by a method of perturbation. We assume that each root can be represented as $\lambda_N = \gamma_N + \delta_N$, where λ_N reduces to γ_N in the absence of tides. When tides are absent, κ vanishes, and Eq. (54) reduces to just

$$0 = \lambda^4 + \lambda^2 + 27M_1M_2/4, \quad (58)$$

equivalent to Eq. (3.141) of Murray and Dermott (1999). Eq. (58) above is a *biquadratic* equation; still quartic, but now a quadratic equation in λ^2 , and much easier to solve for all four roots γ_N .

Solving Eq. (58) by the quadratic formula gives $\gamma_1^2 = \gamma_2^2 = -1/2 - \sqrt{1 - 27M_1M_2}/2$ for the first two roots, and $\gamma_3^2 = \gamma_4^2 = -1/2 + \sqrt{1 - 27M_1M_2}/2$ for the other two roots. Then all four roots are

$$\gamma_1 = \frac{+j}{\sqrt{2}} \sqrt{1 + \sqrt{1 - 27M_1M_2}},$$

$$\gamma_2 = \frac{-j}{\sqrt{2}} \sqrt{1 + \sqrt{1 - 27M_1M_2}},$$

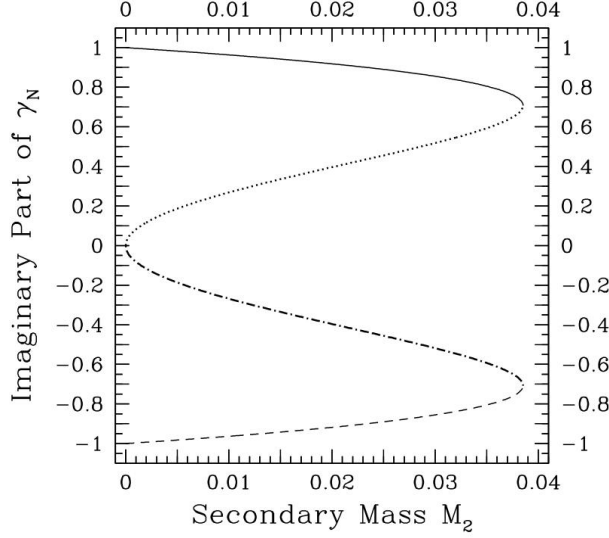


Figure 2: Imaginary parts of γ_1 , γ_2 , γ_3 , and γ_4 as functions of M_2 , the mass of the secondary. Solid curve: $\text{Im}(\gamma_1)$. Dashed curve: $\text{Im}(\gamma_2) = -\text{Im}(\gamma_1)$. Dotted curve: $\text{Im}(\gamma_3)$. Dot-dashed curve: $\text{Im}(\gamma_4) = -\text{Im}(\gamma_3)$.

$$\begin{aligned}\gamma_3 &= \frac{+j}{\sqrt{2}} \sqrt{1 - \sqrt{1 - 27M_1M_2}}, \\ \gamma_4 &= \frac{-j}{\sqrt{2}} \sqrt{1 - \sqrt{1 - 27M_1M_2}},\end{aligned}\quad (59)$$

equivalent to Formulae (3.143) and (3.144) of Murray and Dermott (1999). Note that $\gamma_2 = -\gamma_1$ and $\gamma_4 = -\gamma_3$, while $\gamma_1^2 + \gamma_3^2 = -1$.

If $1 - 27M_1M_2 < 0$ (so $M_2 > (1 - \sqrt{23/27})/2 \approx 0.03852 \approx 1/25.96$; Dobrovolskis, 2013), γ_2 and γ_3 have positive real parts, and the motion is unstable. Otherwise, all four roots are pure imaginary, and γ_1 and γ_2 correspond to harmonic epicyclic motion with a period slightly longer than the orbital period of M_2 around M_1 , while γ_3 and γ_4 correspond to a harmonic libration of still longer period (Murray and Dermott, 1999).

Figure 2 graphs the imaginary parts of γ_1 , γ_2 , γ_3 , and γ_4 as functions of M_2 , for $M_1M_2 \leq 1/27$, from Formulae (59). For $M_2 \ll 0.02$, $\gamma_1 \approx +j\sqrt{1 - 27M_2/4} \approx +j[1 - 27M_2/8]$, $\gamma_2 \approx -j[1 - 27M_2/8]$, $\gamma_3 \approx +\sqrt{-27M_2/4} = +3j\sqrt{3M_2}/2$, and $\gamma_4 \approx -3j\sqrt{3M_2}/2$.

In the two-body case when M_2 vanishes, γ_3 and γ_4 both vanish as well, while $\gamma_1 = +j$ and $\gamma_2 = -j$. (In this special case, the exponential solutions $\exp(\gamma_3 t)$ and $\exp(\gamma_4 t)$ are replaced by secular solutions of the form $D + Et$, where E is now a constant velocity.) At $M_1M_2 = 1/27$ ($M_2 \approx 0.03852$), γ_1 and γ_3 both equal $+j/\sqrt{2}$, while γ_2 and γ_4 both equal $-j/\sqrt{2}$. (In this special case, the solutions take the form $[D + Et]\exp(\gamma_N t)$.)

Now when tides are present, $0 < \kappa \ll 1$, and we assume that each root of Eq. (54) is perturbed to $\lambda_N = \gamma_N + \delta_N$. For the time being, we also presume that δ_N is of the same order as κ . Then Eq. (57) can be expanded as

$$0 = [\gamma_N^4 + 4\gamma_N^3\delta_N] + [\gamma_N^2 + 2\gamma_N\delta_N] + 27M_1M_2/4$$

$$\begin{aligned}
& +\kappa\gamma_N^3\tau[4-107M_1M_2/8]+\kappa\gamma_N^2[-6+137M_1M_2/8] \\
& +\kappa\gamma_N\tau[-3+39M_1M_2/4]+\kappa[-3+687M_1M_2/32],
\end{aligned} \tag{60}$$

to first degree in δ_N and κ .

Subtracting Eq. (58) from Eq. (60) above and solving for δ_N then gives

$$\begin{aligned}
\delta_N & = \kappa\{\gamma_N^3\tau[-4+107M_1M_2/8]+\gamma_N^2[6-137M_1M_2/8] \\
& +\gamma_N\tau[3-39M_1M_2/4]+[3-687M_1M_2/32]\}/[4\gamma_N^3+2\gamma_N].
\end{aligned} \tag{61}$$

Note that Eqs. (60) and (61) above become invalid when γ_N vanishes, as γ_3 and γ_4 do when M_2 vanishes; we avoid this difficulty by finding only δ_1 and δ_2 this way. Eqs. (60) and (61) also become invalid when γ_N^2 approaches -2 , as all four roots do when M_1M_2 approaches $1/27$ ($M_2 \approx 0.03852$). We avoid this issue by treating only $M_2 < \sim 0.03$ henceforth; then all four γ_N are strictly imaginary.

5.4 Epicycles

At this point it is useful to consider the real and imaginary parts of δ_N separately. Because each γ_N is imaginary, the entire denominator of Formula (61) also is imaginary, while the constant, linear, quadratic, and cubic terms of its numerator alternate between real and imaginary. Then the real part of δ_N becomes

$$\text{Re}(\delta_N) = \kappa\tau\{\gamma_N^3[-4+107M_1M_2/8]+\gamma_N[3-39M_1M_2/4]\}/[4\gamma_N^3+2\gamma_N], \tag{62}$$

while its imaginary part becomes

$$\text{Im}(\delta_N) = -j\kappa\{\gamma_N^2[6-137M_1M_2/8]+[3-687M_1M_2/32]\}/[4\gamma_N^3+2\gamma_N]. \tag{63}$$

Note from Formula (62) that the real part of δ_N vanishes when the tidal time lag τ vanishes, as expected for the case with no dissipation. Note also that $4\gamma_1^2+2=4\gamma_2^2+2=-2\sqrt{1-27M_1M_2}$. Then substituting γ_1 into Formula (62) gives

$$\begin{aligned}
\text{Re}(\delta_1) & = \kappa\tau\{[1/2+\sqrt{1-27M_1M_2}/2][4-107M_1M_2/8]+[3-39M_1M_2/4]\}/[-2\sqrt{1-27M_1M_2}] \\
& = \kappa\tau\{[5-263M_1M_2/16]+[2-107M_1M_2/16]\sqrt{1-27M_1M_2}\}/[-2\sqrt{1-27M_1M_2}] \\
& = \kappa\tau\{-1+107M_1M_2/32+[-5/2+263M_1M_2/32]/\sqrt{1-27M_1M_2}\}.
\end{aligned} \tag{64}$$

Likewise, substituting γ_1 into Formula (63) gives

$$\begin{aligned}
\text{Im}(\delta_1) & = \kappa\{[-1/2-\sqrt{1-27M_1M_2}/2][6-137M_1M_2/8]+[3-687M_1M_2/32]\}/\sqrt{2[1-27M_1M_2][1+\sqrt{1-27M_1M_2}]} \\
& = \kappa\{-413M_1M_2/32+[-3+137M_1M_2/16]\sqrt{1-27M_1M_2}\}/\sqrt{2[1-27M_1M_2][1+\sqrt{1-27M_1M_2}]} \\
& = \kappa\{-3+137M_1M_2/16-413M_1M_2[1-27M_1M_2]^{-1/2}/32\}/\sqrt{2+2\sqrt{1-27M_1M_2}}.
\end{aligned} \tag{65}$$

Substituting $\gamma_2 = -\gamma_1$ into Formulae (62) and (63) gives just $\text{Re}(\delta_2) = \text{Re}(\delta_1)$, but $\text{Im}(\delta_2) = -\text{Im}(\delta_1)$. Thus δ_1 and δ_2 are complex conjugates, and so are $\lambda_1 = \gamma_1 + \delta_1$ and $\lambda_2 = \gamma_2 + \delta_2$, as anticipated.

Figure 3 graphs the real and imaginary parts of δ_1 and δ_2 as functions of M_2 from Formulae (64) and (65) above. Note that the vertical scale of Fig. 3 is ten times greater than that of Fig. 2, but that the real parts of δ_1 and δ_2 are normalized by $\kappa\tau$, while their imaginary parts are normalized by just κ . The imaginary parts of δ_1 and δ_2 are not very important, because they only change the epicyclic frequency slightly; but their real parts are very important, because they may determine the stability or instability of the epicycles. Note

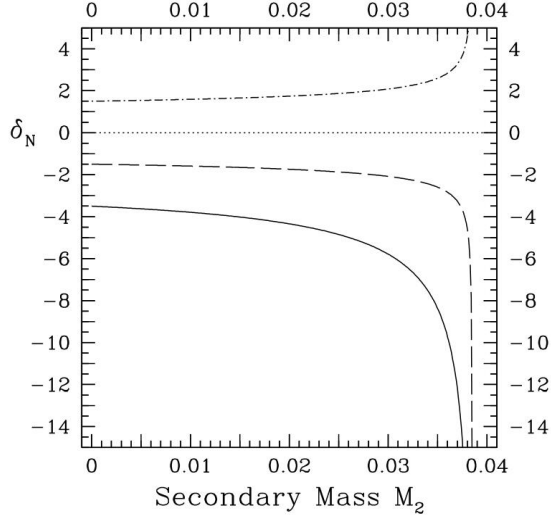


Figure 3: δ_1 and δ_2 as functions of M_2 , the mass of the secondary. Solid curve: $\text{Re}(\delta_1) = \text{Re}(\delta_2)$, normalized by $\kappa\tau$. Dashed curve: $\text{Im}(\delta_1)$, normalized by κ . Dot-dashed curve: $\text{Im}(\delta_2) = -\text{Im}(\delta_1)$. The horizontal dotted line denotes the zero level.

that the real parts of δ_1 and δ_2 are negative for all $M_1M_2 < 1/27$ ($M_2 < \sim 0.03852$), so the epicycles decay exponentially with an e-folding time of $-1/[n\text{Re}(\delta_1)]$.

When M_2 vanishes, as in the two-body problem with tides, $\text{Re}(\delta_1)$ and $\text{Re}(\delta_2)$ reduce to $-7\kappa\tau/2$ from Formula (64), while $\text{Im}(\delta_1) = -\text{Im}(\delta_2)$ reduces to $-3\kappa/2$ from Formula (65). The former agrees with the damping time τ_{AL} from Formula (61) of Couturier *et al.* (2021), when Q of the secondary is set to infinity; our $\text{Re}(\delta_1)$ also agrees with the eccentricity damping time τ_e from Formula 4.198 of Murray and Dermott (1999), where their C_S , $\tilde{\mu}_S$, and Q_S are identified with our R , $3/(2k)$, and $1/(n\tau)$, respectively. Murray and Dermott (1999) also determined that 3/7 of the damping rate arises from radial tides, and 4/7 from transverse tides; however, they used an energy argument inapplicable to problems with more than two bodies. Note that Formulae (64) and (65) cannot be represented as any simple combination of two two-body problems.

5.5 Librations

The above perturbation procedure fails for λ_3 and λ_4 as M_2 approaches zero, because γ_3 and γ_4 both vanish then. However, now that we know two roots $\lambda_1 = \gamma_1 + \delta_1$ and $\lambda_2 = \gamma_2 + \delta_2$ of Eq. (57), we can use them to find its last two roots λ_3 and λ_4 . The quartic Eq. (54) is of the form $0 = \prod_1^4 (\lambda - \lambda_N)$. In principle, we could divide Eq. (57) by its factors $(\lambda - \lambda_1)$ and $(\lambda - \lambda_2)$ to deflate it into a quadratic, namely

$$0 = (\lambda - \lambda_3)(\lambda - \lambda_4) = \lambda^2 - v[\lambda_3 + \lambda_4] + \lambda_3\lambda_4. \quad (66)$$

The coefficients of quadratic equation (66) above are just the sum and product of λ_3 and λ_4 ; so we can use a short-cut to find these coefficients. The constant term on the right-hand side of the quartic Eq. (57) is just $\prod_1^4 \lambda_N = \lambda_1 \lambda_2 \lambda_3 \lambda_4$, while its cubic term is $-v^3 \sum_1^4 \lambda_N$. Thus from Eq. (57), the sum of all four roots λ_N is $\kappa\tau[-4 + 107M_1M_2/8]$, while their product is $27M_1M_2/4 + \kappa[-3 + 687M_1M_2/32]$. When κ vanishes, note from Formulae (59) how the roots γ_N of the biquadratic Eq. (58) satisfy the above, because their sum vanishes, while their product is just $27M_1M_2/4$.

When $\kappa \neq 0$, since we know λ_1 and λ_2 , and we also know $\sum_1^4 \lambda_N$ and $\prod_1^4 \lambda_N$, then we can find the sum and product of λ_3 and λ_4 :

$$\lambda_3 + \lambda_4 = \kappa\tau[-4 + 107M_1M_2/8] - [\lambda_1 + \lambda_2], \quad (67)$$

while

$$\lambda_3\lambda_4 = \{27M_1M_2/4 + \kappa[-3 + 687M_1M_2/32]\} / [\lambda_1\lambda_2]. \quad (68)$$

Because λ_1 and λ_2 are complex conjugates, their sum is just $\lambda_1 + \lambda_2 = \text{Re}(\lambda_1) + \text{Re}(\lambda_2) = \text{Re}(\delta_1) + \text{Re}(\delta_2) = 2 \text{Re}(\delta_1) = 2 \text{Re}(\delta_2)$, while their product is just the square of their magnitudes:

$$\begin{aligned} \lambda_1\lambda_2 &= \text{Re}^2(\lambda_1) + \text{Im}^2(\lambda_1) = \text{Re}^2(\gamma_1 + \delta_1) + \text{Im}^2(\gamma_1 + \delta_1) = [\text{Re}(\gamma_1) + \text{Re}(\delta_1)]^2 + [\text{Im}(\gamma_1) + \text{Im}(\delta_1)]^2 \\ &= \text{Re}^2(\delta_1) + \text{Im}^2(\gamma_1) + 2 \text{Im}(\gamma_1)\text{Im}(\delta_1) + \text{Im}^2(\delta_1) \approx \text{Im}^2(\gamma_1) + 2 \text{Im}(\gamma_1)\text{Im}(\delta_1), \end{aligned} \quad (69)$$

to first degree in κ .

Then the sum of λ_3 and λ_4 is just

$$\lambda_3 + \lambda_4 = \kappa\tau[-4 + 107M_1M_2/8] - 2 \text{Re}(\delta_1) \quad (70)$$

$$\begin{aligned} &\approx \kappa\tau[-4 + 107M_1M_2/8] - \kappa\tau\{-2 + 107M_1M_2/16 + [-5 + 263M_1M_2/16]/\sqrt{1 - 27M_1M_2}\} \\ &= \kappa\tau\{-2 + 107M_1M_2/16 + [5 - 263M_1M_2/16]/\sqrt{1 - 27M_1M_2}\}, \end{aligned}$$

while their product is

$$\lambda_3\lambda_4 \approx \frac{27M_1M_2/4 + \kappa[-3 + 687M_1M_2/32]}{\text{Im}^2(\gamma_1) + 2 \text{Im}(\gamma_1)\text{Im}(\delta_1)} \quad (71)$$

$$\begin{aligned} &\approx \{27M_1M_2/4 + \kappa[-3 + 687M_1M_2/32]\} [\text{Im}^2(\gamma_1) - 2 \text{Im}(\gamma_1)\text{Im}(\delta_1)] / \text{Im}^4(\gamma_1) \\ &= [1 + \sqrt{1 - 27M_1M_2} - \kappa\{-6 + 137M_1M_2/8 - 413M_1M_2[1 - 27M_1M_2]^{-1/2}/16\}] \\ &\quad \{27M_1M_2/4 + \kappa[-3 + 687M_1M_2/32]\} / [1 - 27M_1M_2/2 + \sqrt{1 - 27M_1M_2}] \\ &\approx \{27M_1M_2[1 + \sqrt{1 - 27M_1M_2}]/4 + \kappa[27M_1M_2\{6 - 137M_1M_2/8 - 413M_1M_2[1 - 27M_1M_2]^{-1/2}/16\}/4] \\ &\quad + \kappa[-3 + 687M_1M_2/32][1 + \sqrt{1 - 27M_1M_2}]\} / [1 - 27M_1M_2/2 + \sqrt{1 - 27M_1M_2}], \end{aligned}$$

again to first degree in κ .

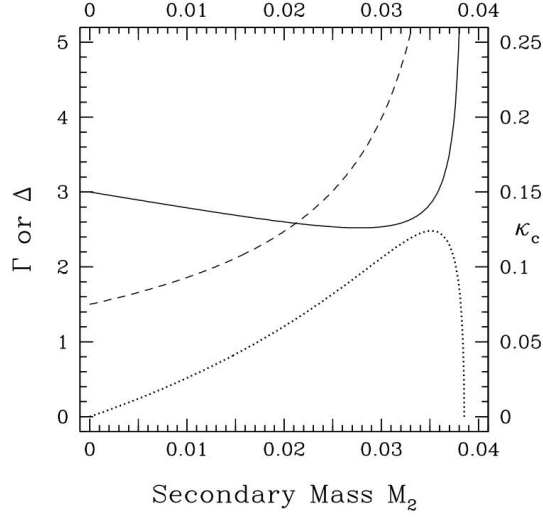


Figure 4: Left-hand scale: Γ (solid curve) and Δ (dashed curve) as functions of M_2 , the mass of the secondary. Right-hand scale: κ_c (dotted curve) as a function of M_2 .

Note that $\lambda_3 + \lambda_4$ from Formula (70) is proportional to $\kappa\tau$, while $\lambda_3\lambda_4$ from Formula (71) above is linear in κ . Thus to first degree in κ , Formula (66) reduces to just

$$\lambda \approx [\lambda_3 + \lambda_4]/2 \pm \sqrt{-\lambda_3\lambda_4} \equiv \kappa\tau\Delta \pm \sqrt{\gamma_3^2 + \kappa\Gamma}, \quad (72)$$

where

$$\Delta = -1 + 107M_1M_2/32 + [5/2 - 263M_1M_2/32]/\sqrt{1 - 27M_1M_2} \quad (73)$$

and

$$\Gamma = (27M_1M_2\{-6 + 137M_1M_2/8 + 413M_1M_2[1 - 27M_1M_2]^{-1/2}/16\})/4 \quad (74)$$

$$+ [3 - 687M_1M_2/32][1 + \sqrt{1 - 27M_1M_2}]/(1 - 27M_1M_2/2 + \sqrt{1 - 27M_1M_2}).$$

Figure 4 graphs Γ and Δ as functions of M_2 . Note how Δ reduces to $3/2$ for the two-body case $M_2 = 0$, but increases monotonically with M_2 , until it becomes infinite at $M_1M_2 = 1/27 \approx 0.037037$ ($M_2 \approx 0.03852$). In contrast, Γ reduces to 3 for $M_2 = 0$, decreases to a shallow minimum of ~ 2.5215 at $M_2 \approx 0.0278$, and then increases again to infinity at $M_1M_2 = 1/27$.

Because γ_3^2 is negative, while Γ and Δ both are positive, γ_3^2 represents the stabilizing influence of the secondary mass M_2 in Formula (72) for λ , while $\kappa\Gamma$ and $\kappa\tau\Delta$ represent the destabilizing influences of the tidal force and of tidal dissipation, respectively.

Note that $\sqrt{\gamma_3^2 + \kappa\Gamma}$ in Formula (72) vanishes when κ reaches a critical value $\kappa_c \equiv -\gamma_3^2/\Gamma$. Figure 4 also graphs κ_c as a function of M_2 , on a vertical scale 20 times smaller than Γ and Δ . Note how κ_c rises from zero at $M_2 = 0$ to a peak of ~ 0.1241 at $M_2 \approx 0.0351$, but then falls to zero again at $M_1M_2 = 1/27$.

For $\kappa > \kappa_c$, the square root in Formula (72) is positive, and the Lagrange points $L'4$ and $L'5$ are unstable. For $\kappa < \kappa_c$, the square root in Formula (72) becomes imaginary, and λ represents a slowly-growing libration with a period of $2\pi/\sqrt{-\gamma_3^2 - \kappa\Gamma}$ and an e-folding time of $1/(\kappa\tau\Delta)$. When tides from the secondary are

neglected, Δ reduces to $3/2$, so the e-folding time of the libration becomes $2/(3\kappa\tau)$. This agrees with the e-folding time $\tau_{\text{lib}} = 7\tau_{\text{AL}}/3$ from Formula (61) of Couturier *et al.* (2021), when tides in the secondary are neglected.

5.6 Complete solution

The general solution to System (23) and (24) is of the form

$$x = x' + \alpha_1 \exp(\lambda_1 t) + \alpha_2 \exp(\lambda_2 t) + \alpha_3 \exp(\lambda_3 t) + \alpha_4 \exp(\lambda_4 t), \quad (75)$$

$$y = y' + \beta_1 \exp(\lambda_1 t) + \beta_2 \exp(\lambda_2 t) + \beta_3 \exp(\lambda_3 t) + \beta_4 \exp(\lambda_4 t), \quad (76)$$

where the constant coefficients α_N and β_N are complex amplitudes.

To evaluate these constants, first differentiate solutions (75) and (76) above:

$$\dot{x} = \alpha_1 \lambda_1 \exp(\lambda_1 t) + \alpha_2 \lambda_2 \exp(\lambda_2 t) + \alpha_3 \lambda_3 \exp(\lambda_3 t) + \alpha_4 \lambda_4 \exp(\lambda_4 t), \quad (77)$$

$$\dot{y} = \beta_1 \lambda_1 \exp(\lambda_1 t) + \beta_2 \lambda_2 \exp(\lambda_2 t) + \beta_3 \lambda_3 \exp(\lambda_3 t) + \beta_4 \lambda_4 \exp(\lambda_4 t). \quad (78)$$

Then setting Formulae (75) through (78) above respectively equal to the initial conditions $x = x' + x_0$, $y = y' + y_0$, $\dot{x} = \dot{x}_0$, and $\dot{y} = \dot{y}_0$ at time $t = 0$ gives $\sum \alpha_N = x_0$, $\sum \beta_N = y_0$, $\sum \alpha_N \lambda_N = \dot{x}_0$, and $\sum \beta_N \lambda_N = \dot{y}_0$, as in Formulae (3.127) of Murray and Dermott (1999).

This appears to leave us with four linear equations in eight unknowns, but substituting Formulae (75) through (78) (along with their next derivatives \dot{x} and \dot{y}) into Eqs. (23) and (24) gives two relations between α_N and β_N for each N :

$$\beta_N / \alpha_N = \frac{\lambda_N^2 - 3/4 - \kappa[1 - 9M_1 M_2 / 8] - \kappa\tau[93M_1 M_2 / 16 - 3/2]\lambda_N}{2\lambda_N \pm 3\sqrt{3}(M_1 - M_2)/4 \pm \kappa\sqrt{3}(M_1 - M_2)(2 - \lambda_N \tau/2)} \equiv q_N \quad (79)$$

and

$$\beta_N / \alpha_N = \frac{-2\lambda_N \pm 3\sqrt{3}(M_1 - M_2)/4 \pm \kappa\sqrt{3}(M_1 - M_2)(2 - \lambda_N \tau/2)}{\lambda_N^2 - 9/4 - \kappa(5 - 16M_1 M_2) - \kappa(121M_1 M_2 - 5/2)\lambda_N \tau} \equiv q'_N. \quad (80)$$

Actually the complex quotients q_N and q'_N from Formulae (79) and (80) above are equal by Eqs. (56) and (57).

Then the final system for the initial conditions takes the pleasing form

$$\begin{bmatrix} 1 & 1 & 1 & 1 \\ \lambda_1 & \lambda_2 & \lambda_3 & \lambda_4 \\ q_1 & q_2 & q_3 & q_4 \\ q_1 \lambda_1 & q_2 \lambda_2 & q_3 \lambda_3 & q_4 \lambda_4 \end{bmatrix} \cdot \begin{bmatrix} \alpha_1 \\ \alpha_2 \\ \alpha_3 \\ \alpha_4 \end{bmatrix} = \begin{bmatrix} x_0 \\ \dot{x}_0 \\ y_0 \\ \dot{y}_0 \end{bmatrix}. \quad (81)$$

System (81) above can be solved numerically for any set of initial conditions x_0 , y_0 , \dot{x}_0 , \dot{y}_0 , and parameters M_2 , κ , τ .

Furthermore, it is possible to express x and y entirely in terms of real quantities. Note that λ_1 and λ_2 , q_1 and q_2 , α_1 and α_2 , β_1 and β_2 all are complex conjugate pairs; likewise, λ_3 and λ_4 , q_3 and q_4 , α_3 and α_4 , β_3 and β_4 all are complex conjugate pairs as well. Thus $\alpha_1 = A_1 + ja_1$, $\alpha_2 = A_1 - ja_1$, $\alpha_3 = A_3 + ja_3$, and $\alpha_4 = A_3 - ja_3$, where $A_1 = \text{Re}(\alpha_1)$, $a_1 = \text{Im}(\alpha_1)$, $A_3 = \text{Re}(\alpha_3)$, and $a_3 = \text{Im}(\alpha_3)$. Similarly, we write $\beta_1 = B_1 + jb_1$, $\beta_2 = B_1 - jb_1$, $\beta_3 = B_3 + jb_3$, and $\beta_4 = B_3 - jb_3$, where $B_1 = \text{Re}(\beta_1)$, $b_1 = \text{Im}(\beta_1)$, $B_3 = \text{Re}(\beta_3)$, and $b_3 = \text{Im}(\beta_3)$.

Finally, $\lambda_1 = \Lambda_1 + j\ell_1$, $\lambda_2 = \Lambda_1 - j\ell_1$, $\lambda_3 = \Lambda_3 + j\ell_3$, and $\lambda_4 = \Lambda_3 - j\ell_3$. Here $\Lambda_1 = \text{Re}(\lambda_1) = \text{Re}(\delta_1)$ is the decay rate of μ 's eccentric epicycles, while $\ell_1 = \text{Im}(\lambda_1) = \text{Im}(\gamma_1 + \delta_1)$ is their angular frequency. Likewise, $\Lambda_3 = \text{Re}(\lambda_3) = \kappa\tau\Delta$ is the growth rate of μ 's tadpole librations, while $\ell_3 = \text{Im}(\lambda_3) = \sqrt{-\gamma_3^2 - \kappa\Gamma}$ is their angular frequency.

Formulae (75) and (76) can be expressed in terms of real quantities as

$$\begin{aligned} x &= x' + \exp(\Lambda_1 t)[(\alpha_1 + \alpha_2) \cos(\ell_1 t) + (\alpha_1 - \alpha_2) j \sin(\ell_1 t)] + \exp(\Lambda_3 t)[(\alpha_3 + \alpha_4) \cos(\ell_3 t) + (\alpha_3 - \alpha_4) j \sin(\ell_3 t)] \\ &= x' + \exp(\Lambda_1 t)[2A_1 \cos(\ell_1 t) - 2a_1 \sin(\ell_1 t)] + \exp(\Lambda_3 t)[2A_3 \cos(\ell_3 t) - 2a_3 \sin(\ell_3 t)] \end{aligned} \quad (82)$$

and

$$\begin{aligned} y &= y' + \exp(\Lambda_1 t)[(\beta_1 + \beta_2) \cos(\ell_1 t) + (\beta_1 - \beta_2) j \sin(\ell_1 t)] + \exp(\Lambda_3 t)[(\beta_3 + \beta_4) \cos(\ell_3 t) + (\beta_3 - \beta_4) j \sin(\ell_3 t)] \\ &= y' + \exp(\Lambda_1 t)[2B_1 \cos(\ell_1 t) - 2b_1 \sin(\ell_1 t)] + \exp(\Lambda_3 t)[2B_3 \cos(\ell_3 t) - 2b_3 \sin(\ell_3 t)]. \end{aligned} \quad (83)$$

For example, Table 4 lists the numerical results for the above quantities for several different parameter sets, but all with a fairly heavy secondary mass $M_2 = 0.01$, comparable to the Moon/Earth mass ratio. Then $\Delta \approx 1.858\,680$, $\Gamma \approx 2.789\,128$, $\kappa_c \approx 0.025\,818\,3$, and the secondary's dimensionless Hill radius is $(M_2/3)^{1/3} \approx 0.149\,380$. Furthermore, we chose initial conditions $x_0 = y_0 = 10^{-5}$ and $\dot{x}_0 = \dot{y}_0 = 0$ in each case.

Case 1 is the standard CR3BP without tides, when κ vanishes and τ is irrelevant. Murray and Dermott (1999, p. 92) did the same case; for comparison, Table 4 lists the values they reported as ‘‘Case 0’’. Note that Cases 0 and 1 agree to the given precision.

Case 2 in Table 4 lists the results for the same parameters, except now with tides of large dimensionless magnitude $\kappa = 0.000\,1$, but still no dissipation. Case 3 lists the results for tides of the same magnitude, but now with weak dissipation, for a dimensionless time lag $\tau = 0.01$ ($Q \approx 100$), appropriate for a ‘‘dry’’ planet like the Moon or Mars. Case 4 lists the results for tides of the same magnitude again, but now with strong dissipation, for a dimensionless time lag $\tau = 0.10$ ($Q \approx 10$), appropriate for a ‘‘wet’’ planet like the Earth. In each of these cases, the tabulated λ_N found by perturbing γ_N agree with those found more directly by solving the quartic equation (57) numerically.

The e-folding rates ζ and Λ_N all vanish in Cases 1 and 2 without dissipation, so m_o maintains quasi-periodic vertical oscillations, eccentric epicycles, and tadpole librations indefinitely. In Case 3 with weak dissipation, the vertical oscillations decay slowly with an e-folding time of $\sim 320\,000$ orbital periods, while the epicycles decay quickly with an e-folding time of only $\sim 42\,000$ orbits; however, the tadpole librations grow, with an intermediate e-folding time of $\sim 86\,000$ orbits. In Case 4 with strong dissipation, the same things happen, but ten times faster. Thus Cases 3 and 4 with tidal dissipation both are unstable.

Table 4. Numerical results. In all cases, $M_2 = 0.01$, $x_0 = y_0 = 10^{-5}$, and $\dot{x}_0 = \dot{y}_0 = 0$.

Case	0	1	2	3	4
κ	0	0	0.000 1	0.000 1	0.000 1
τ	0	0	0	0.01	0.10
Q	∞	∞	∞	~ 100	~ 10
$1/(2\pi\zeta)$.	∞	∞	-321 493.	-32 149.3
ζ	.	0	0	-0.000 000 495 050	-0.000 004 950 50
η	.	1	1.000 048 637 6	1.000 048 637 6	1.000 048 637 6
x'	.	0	0.000 044 916 7	0.000 044 916 7	0.000 044 916 7
y'	.	0	0.000 012 028 1	0.000 012 028 1	0.000 012 028 1
δ_1	.	0	-0.000 159 059 <i>j</i>	-0.000 003 792 47 -0.000 159 059 <i>j</i>	-0.000 037 924 7 -0.000 159 059 <i>j</i>
$1/(2\pi\Lambda_1)$.	∞	∞	-41 966.0	-4 196.60
Λ_1	.	0	0	-0.000 003 792 47	-0.000 037 924 7
ℓ_1	0.963	0.963 322	0.963 163	0.963 163	0.963 163
$1/(2\pi\Lambda_3)$.	∞	∞	85 627.9	8 562.79
Λ_3	.	0	0	0.000 001 858 68	0.000 018 586 8
ℓ_3	0.268	0.268 348	0.267 828	0.267 828	0.267 828
q_1	.	-0.400 586 +0.606 246 <i>j</i>	-0.400 670 +0.606 112 <i>j</i>	-0.400 672 +0.606 113 <i>j</i>	-0.400 685 +0.606 121 <i>j</i>
q_3	.	-0.548 257 +0.231 134 <i>j</i>	-0.548 355 +0.230 666 <i>j</i>	-0.548 353 +0.230 665 <i>j</i>	-0.548 340 +0.230 663 <i>j</i>
$q_1\lambda_1$.	-0.584 010 -0.385 893 <i>j</i>	-0.583 785 -0.385 911 <i>j</i>	-0.583 784 -0.385 914 <i>j</i>	-0.583 778 -0.385 948 <i>j</i>
$q_3\lambda_3$.	-0.062 024 3 -0.147 123 <i>j</i>	-0.061 778 6 -0.146 865 <i>j</i>	-0.061 779 6 -0.146 864 <i>j</i>	-0.061 788 1 -0.146 856 <i>j</i>
$10^5\alpha_1$.	-1.223 77 +4.272 53 <i>j</i>	-1.223 92 +4.274 37 <i>j</i>	-1.223 89 +4.274 44 <i>j</i>	-1.223 35 +4.274 47 <i>j</i>
$10^5\alpha_3$.	1.723 77 -15.337 6 <i>j</i>	1.723 92 -15.371 5 <i>j</i>	1.723 89 -15.371 7 <i>j</i>	1.723 35 -15.371 6 <i>j</i>
$10^5\beta_1$.	-2.099 98 -2.453 42 <i>j</i>	-2.100 36 -2.454 44 <i>j</i>	-2.100 42 -2.454 46 <i>j</i>	-2.100 67 -2.454 21 <i>j</i>
$10^5\beta_3$.	2.599 97 +8.807 37 <i>j</i>	2.600 36 +8.826 69 <i>j</i>	2.600 41 +8.826 76 <i>j</i>	2.600 68 +8.826 38 <i>j</i>
$2A_1 \times 10^5$	-2.45	-2.447 54	-2.447 84	-2.447 78	-2.446 70
$-2a_1 \times 10^5$	-8.55	-8.545 06	-8.548 74	-8.548 88	-8.548 94
$2A_3 \times 10^5$	3.45	3.447 54	3.447 84	3.447 78	3.446 70
$-2a_3 \times 10^5$	30.7	30.675 2	30.743 0	30.743 4	30.743 2
$2B_1 \times 10^5$	-4.20	-4.199 96	-4.200 72	-4.200 84	-4.201 34
$-2b_1 \times 10^5$	4.90	4.906 84	4.908 88	4.908 92	4.908 42
$2B_3 \times 10^5$	5.20	5.199 94	5.200 72	5.200 82	5.201 36
$-2b_3 \times 10^5$	-17.6	-17.614 74	-17.653 38	-17.653 52	-17.652 76

To illustrate, the loopy trajectory in Fig. 5 plots our analytic solution for Case 1 during the first 12.5 orbital periods P of M_2 around M_1 . Compare Fig. 5 with Fig. 3.15 of Murray and Dermott (1999, p. 96) for Case 0; they agree in essentially every detail. For this length of time, the solutions for Cases 2, 3, and 4 with tides are almost indistinguishable from Case 1 without tides; slight differences on the order of 10^{-5} or less appear to be due mainly to higher-degree terms in κ .

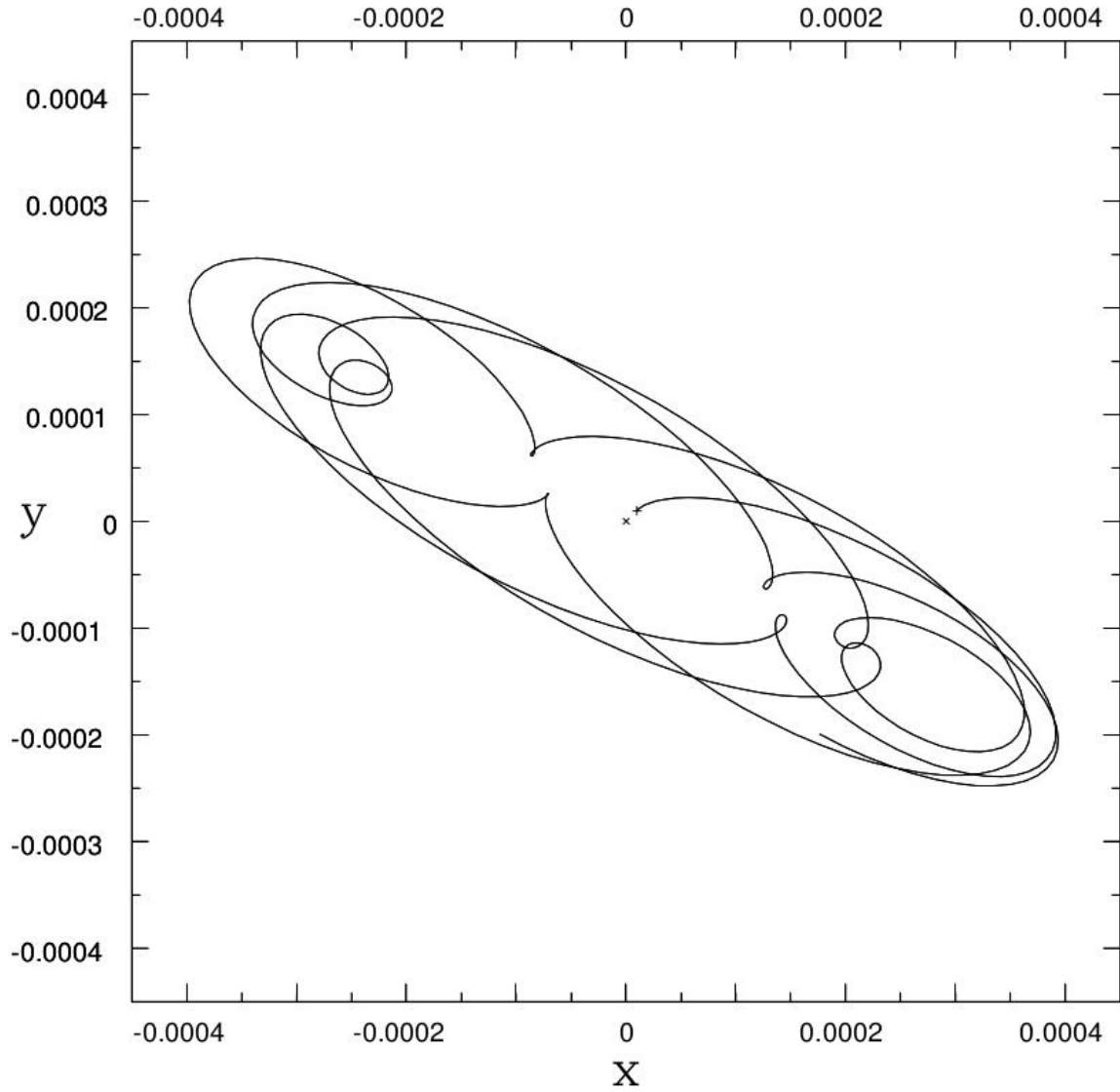


Figure 5: Our analytic solution for Case 1 without tides during the first 12.5 orbital periods of the secondary. x and y are the horizontal deviations from the leading equilateral Lagrange point L_4 . The \times marks the origin, at L_4 , while the $+$ marks the initial location of m_2 . Compare with Fig. 3.15 of Murray and Dermott (1999, p. 96).

6 Numerical Simulations of the Non-Linearized Problem

In order to overcome some limitations of our analytic approach (particularly the assumption of small x and y), we numerically integrated the non-linearized System (1) through (3) (with Formulae 104 through 107 from the Appendix for the tidal forces) for Cases 1 through 4 of Table 4. In each case, we neglected the obliquity ε of m_o , for simplicity; and we set $z_0 = 10^{-6}$ and $\dot{z}_0 = 0$, just to verify the stability of the vertical oscillations; these oscillations are too small to test their coupling with the horizontal motion.

We used the Bulirsch-Stoer integrator “bsstep” (Press *et al.*, 1992) for each simulation, with a tolerance “eps” of 10^{-9} and an initial stepsize of $1/40$ of the orbit period P of M_2 (9° of its mean anomaly). We ran each simulation for one million orbits of M_2 , or until a close encounter occurred.

Our numerical simulation for the first 12.5 periods of Case 1 (no tides) is plotted in Fig. 5, on top of our analytic solution. On this scale, the two solutions are indistinguishable. As a further check, we computed the Jacobi constant C_J from Formula (9) at each time step; its initial value of 3.000 000 000 555 361 was conserved up to the final digit for the entire million periods.

Panel A of Fig. 6 plots our numerical simulation of Case 1 during the first 100 orbital periods P of M_2 , while Panel B plots it for the final 100 P (periods 999 900 through 1 000 000). Although Panels A and B differ in details, the general character and boundary of the trajectory have not changed over a million periods.

In both Panels A and B of Fig. 6, the red ellipses with semi-major axis 0.000 157 200 8, semi-minor axis 0.000 013 647 8, and slope $-29.748\ 130$ graph an analytic approximation to the zero-velocity curve $C_J = 2U + X^2 + Y^2 + M_1M_2$, defined implicitly by setting $\dot{X} = \dot{Y} = \dot{Z} = 0$ in Formula (9) for the Jacobi constant. Note that μ can never cross a zero-velocity curve, or its speed would become imaginary! Note also how the trajectory in Panels A and B never crosses the red ellipses, although it “bounces” off of them at times, when its speed momentarily vanishes.

For comparison, Panel C of Fig. 6 plots our numerical simulation of Case 2 (dissipationless tides) during the first 100 P , while Panel D plots it for the final 100 P . Again, Panels C and D differ in details, but the general character and boundary of the trajectory still do not change over a million periods, because in this case the tides are conservative ($\tau = 0$); even though the Jacobi constant C_J and corresponding zero-velocity curve do not exist, at least not in the simple form given by Formula (9). The main effect of conservative tides is to shift the equilibria slightly away from the equilateral points L4 and L5, to L'4 and L'5.

Figure 7 plots our numerical simulation of Case 3 with weak tidal dissipation ($\tau = 0.01$) in six stages. Panel A plots the first 100 P , in a format like Fig. 6; and in fact the results look very similar. Panel B plots periods 20 000 through 20 100, on the same scale as Panel A; note how the eccentric epicycles have damped considerably, as expected, while the tadpole librations have grown. Panel C plots periods 200 000 through 200 100, on a scale ten times larger, while Panel D plots periods 400 000 through 400 100, on a scale ten times larger still; in both cases, the eccentric epicycles have damped away to insignificance, while the tadpole librations have grown exponentially.

Panel E of Fig. 7 plots our numerical simulation of Case 3 for $t = 600\ 000\ P$ through $600\ 100\ P$, on a shifted scale again ten times larger than Panel D. By this time, the tadpole librations have grown by another order of magnitude, and taken on a peculiar shape which resembles a banana more than a polliwog. Finally, Panel F plots periods 600 100 through 602 999, on a scale about three times larger than Panel E. Note that the primary mass M_1 resides at $x - x' \approx -0.500\ 044\ 916\ 7$, $y - y' \approx -0.866\ 037\ 431\ 9$, marked by the \times on the left, while the secondary mass M_2 resides at $x - x' \approx 0.499\ 955\ 083\ 3$, $y - y' \approx -0.866\ 037\ 431\ 9$, marked by the \times on the right. At $t \approx 602\ 996\ P$, m_o escapes the banana orbit and assumes an eccentric orbit inferior to M_2 . (Recall that $M_2 = 0.01$, so horseshoe orbits are unstable even if dissipation can be neglected; Cuk *et al.*, 2012.) Only about three periods later, at $t \approx 602\ 999\ P$, m_o has a close encounter with the secondary M_2 ($r_2 \approx 0.000\ 861\ 403$; the final time-step is not plotted), and the integrator stops.

For comparison, Fig. 8 plots our numerical simulation of Case 4 with strong tidal dissipation ($\tau = 0.10$) in the same format as Fig. 7, and indeed the results do not look very different. Panels A through E look very similar to those of Fig. 7, except that everything happens about ten times faster; Panel A plots periods 0 through 100, while Panel B plots periods 2 000 through 2 100, Panel C plots periods 20 000 through 20 100, Panel D plots periods 40 000 through 40 100, and Panel E plots periods 60 000 through 60 100. By $t = 60\ 000\ P$, the tadpole librations have taken the peculiar banana-like shape previously seen in Fig. 7.

Panel F of Fig. 8 plots Case 4 for periods 60 100 through 60 327. At $t \approx 61\ 323\ P$, m_o escapes the banana orbit and assumes a tidally decaying eccentric orbit inferior to M_2 . Only about four periods later, at $t \approx 61\ 327\ P$, m_o has a close encounter with the primary M_1 this time ($r_1 \approx 0.047\ 711\ 1$; the final time-step is not plotted), and the integrator stops. The polygonal appearance of the final orbit in Fig. 8 is not due to the integrator, but is an artefact of the discrete output steps.

Certain processes lead to asymmetry between the leading and trailing Trojan points L'4 and L'5, while others do not; for example, radiation pressure is symmetric, but Poynting-Robertson drag is not. Our for-

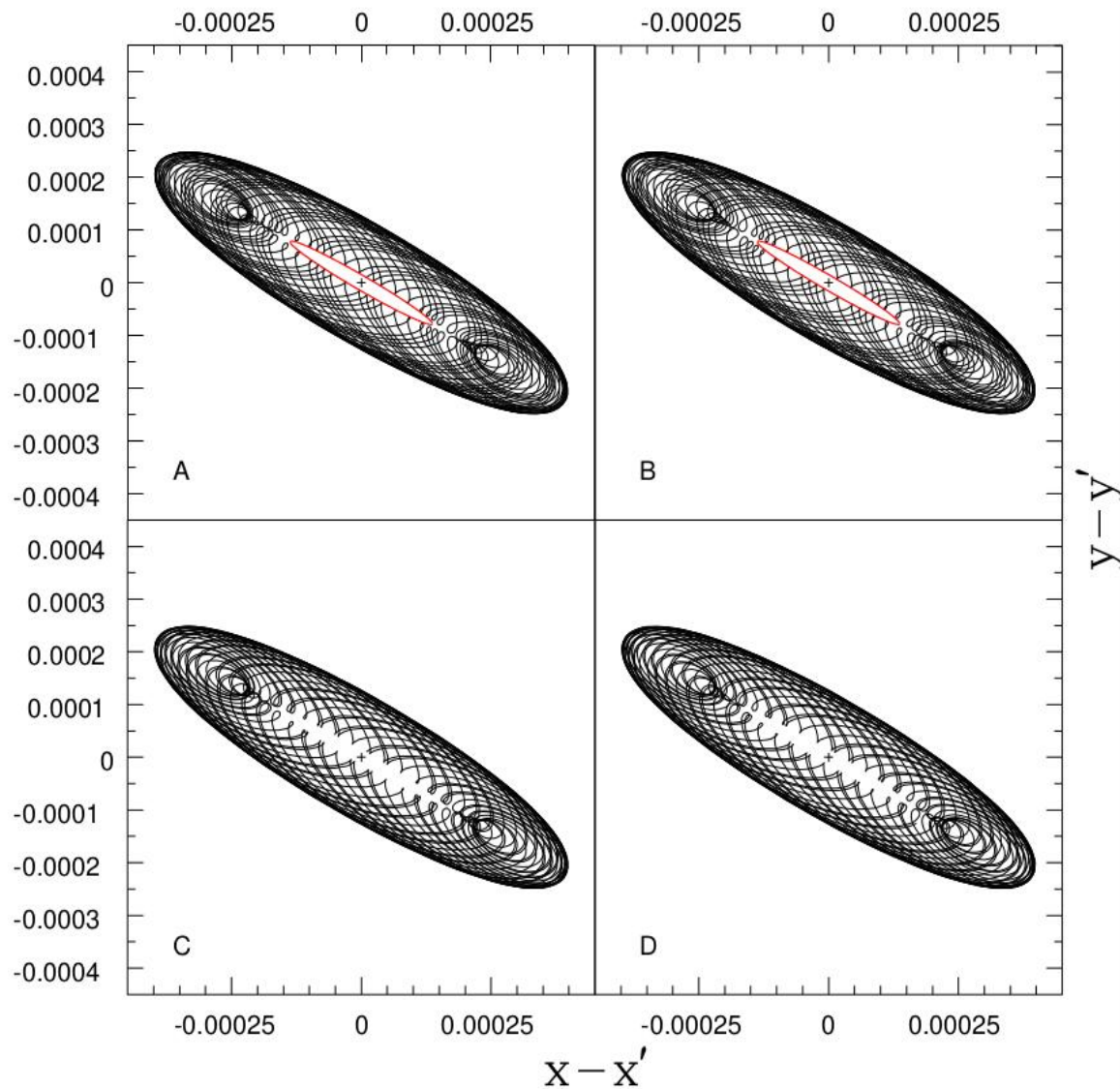


Figure 6: Panel A: Numerical simulation of Case 1 during the first 100 orbital periods P of the secondary. Panel B: Numerical solution for Case 1 during the final 100 P . The plus signs in both A and B mark the origin, at L_4 , while the red ellipses plot the zero-velocity curves corresponding to the Jacobi constant C_J . Panel C: Numerical solution of Case 2 during the first 100 P . Panel D: Numerical solution of Case 2 during the final 100 P . $x - x'$ and $y - y'$ are the horizontal deviations from the leading equilateral Lagrange point L_4 . The plus signs in both C and D mark the origin, at L_4 .

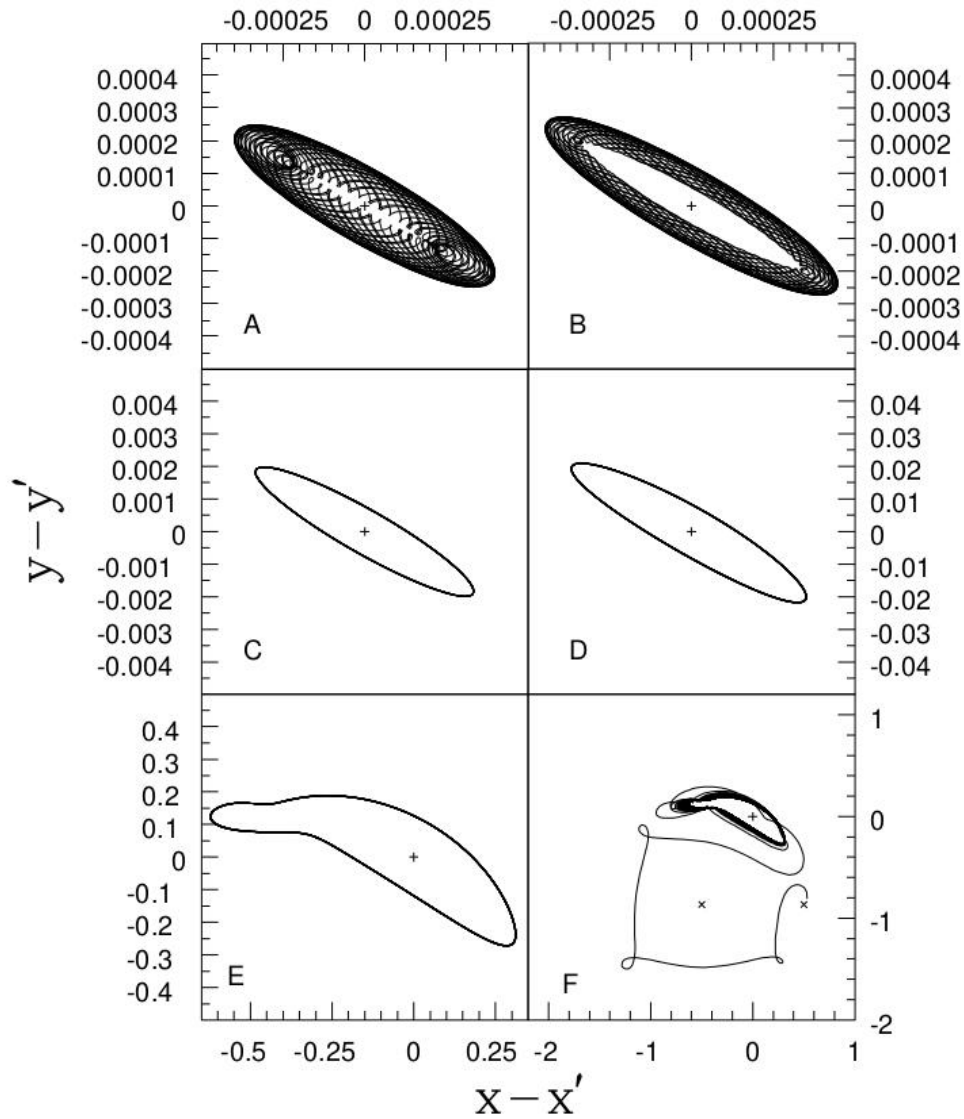


Figure 7: Numerical simulation of Case 3 (weak tidal dissipation). Panel A: The first 100 orbital periods P of M_2 . Panel B: $t = 20\,000 P$ through $20\,100 P$. Panel C: $t = 200\,000 P$ through $200\,100 P$. Panel D: $t = 400\,000 P$ through $400\,100 P$. Panel E: $t = 600\,000 P$ through $600\,100 P$. Panel F: $t = 600\,100 P$ through $602\,999 P$. $x - x'$ and $y - y'$ are the horizontal deviations from the leading equilateral Lagrange point $L/4$. Note different scales in each panel. In Panel F, the \times on the left-hand side marks the location of M_1 , while the \times on the right marks the location of M_2 . The plus signs in each panel mark the origin, at $L/4$.

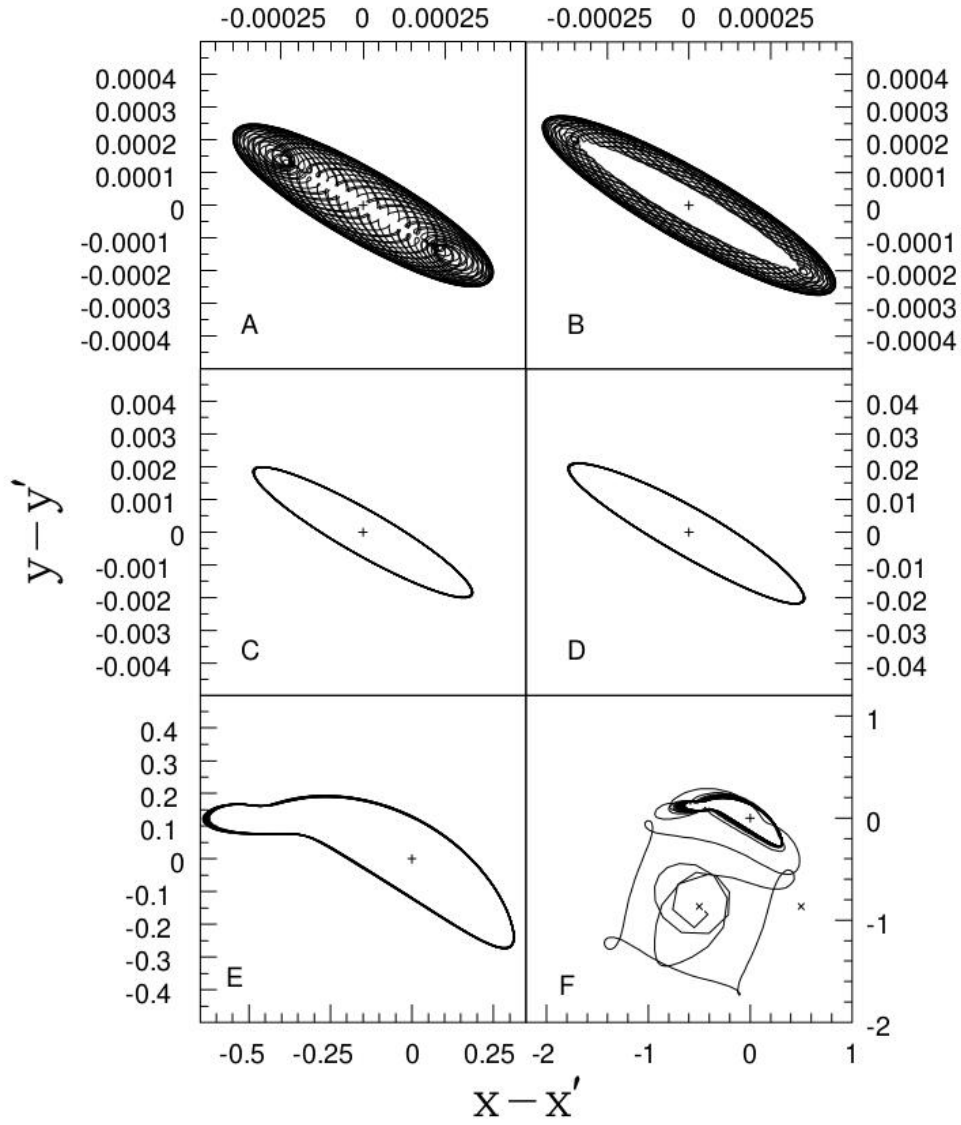


Figure 8: Numerical simulation of Case 4 (strong tidal dissipation). Panel A: The first 100 orbital periods P of M_2 . Panel B: $t = 2\,000 P$ through $2\,100 P$. Panel C: $t = 20\,000 P$ through $20\,100 P$. Panel D: $t = 40\,000 P$ through $40\,100 P$. Panel E: $t = 60\,000 P$ through $60\,100 P$. Panel F: $t = 60\,100 P$ through $61\,327 P$. $x - x'$ and $y - y'$ are the horizontal deviations from the leading equilateral Lagrange point $L'4$. Note different scales in each panel. In Panel F, the polygonal appearance of the final orbit is not due to the integrator, but to the discrete output steps; and the \times on the left-hand side marks the location of M_1 , while the \times on the right marks the location of M_2 . The plus signs in each panel mark the origin, at $L'4$.

mulation of tides is symmetric, so that L'4 and L'5 should be equivalent. When Y is replaced by $-Y$ in Formulae (1) through (8), (23) through (25), and (35) through (37), then Formulae (2), (7), (24), and (36) for \ddot{Y} , $\partial U/\partial Y$, \dot{y} , and f_Y change sign; but their X and Z counterparts are unaffected. In order to demonstrate this symmetry, we also simulated an extra Case 5, identical to Case 4, except starting with $x_0 = -y_0 = 10^{-5}$ from the shifted trailing Lagrange point L'5, rather than $x_0 = y_0 = 10^{-5}$ from the shifted leading Lagrange point L'4.

Figure 9 plots the results of Case 5, in a similar format to Fig. 8 for Case 4, except for changes of scale. Except for the flip of the y axis, panels A through E of Fig. 9 are nearly identical to those of Fig. 8; but as shown in Panel F of Fig. 9, after escaping the banana orbit at $t \approx 60\,324 P$, now m_o assumes an eccentric orbit superior to M_2 . About nine periods later, at $t \approx 60\,333 P$, m_o has a close encounter with the secondary M_2 ($r_2 \approx 0.015\,045\,7$; the final time-step is not plotted), and the integrator stops. Except for the flip of the y axis, we attribute the minor differences between Cases 4 and 5 to numerical noise and/or chaos.

Finally, in Cases 1 and 2, the Z component of motion showed nearly harmonic oscillations for the entire simulation, with a period nearly equal to unity, as expected. In contrast, Cases 3 through 5 experienced a simple exponential decay of the vertical oscillations until the end, with the time constants approximately as given in Table 4, practically uncoupled from the horizontal motion in X and Y .

7 Discussion

We have found analytic solutions for the motion of a small planet near the Trojan point L4 or L5 of a more massive planet, including the effects of tides in the small planet. Our analytic results include Formula (64) for the decay rate of the small planet's eccentric epicycles, and Formula (73) for the growth rate of its tadpole librations, which agree with those of Couturier *et al.* (2021). Thus we confirm their conclusion that dissipation of energy by tides in a Trojan planet tends to destabilize its orbit. We also confirm this analytic conclusion by several numerical simulations.

The vast majority of known exoplanets that have been observed transiting their host star have orbital periods of a few months or less, so they and any co-orbital companions may well be subjected to strong tidal forces. Therefore such planets may not survive for long times, which may explain why no Trojan planets have yet been discovered by *Kepler*, *TESS*, or other searches.

If tidal forces are responsible for removing co-orbital companions from these planets (rather than such configurations being absent at the end of the planet formation era), then smaller Trojan planets and those with longer orbital periods may begin to turn up over longer periods of observation. The tidal properties of water-rich sub-Neptune exoplanets may differ substantially from those predicted by dry gas-rich models. Thus, future detection of a population of Trojan companions may help elucidate the internal structure of exoplanets that are unlike any of their Solar System cousins.

Our conclusion that tides destabilize the orbits of Trojan planets may be altered by relaxing some of the assumptions in our model. For example, we have neglected any eccentricity of the secondary's orbit around the primary. Many known exoplanets are in quite eccentric orbits; but note that Trojans are even less stable in such systems.

We also have neglected tides in the primary and secondary. Tides in the primary are certainly important in many planet/satellite systems; but as distances between bodies are generally larger in the context of exoplanets, and stars tend to be less tidally dissipative than even giant planets, tides in stars are less likely to be important, except for planets on very eccentric or very short-period orbits.

We have neglected the mass m_o of the Trojan as well; its influence on the primary and secondary might lead to interesting and possibly observable behaviors. We may revisit this question in future work.

Similarly, a significant obliquity ε of Trojans or their non-synchronous rotation might affect our results. Of still greater concern, the Appendix discusses the possible frequency dependence of τ or Q ; in other contexts, different frequency dependences can lead to different behaviors.

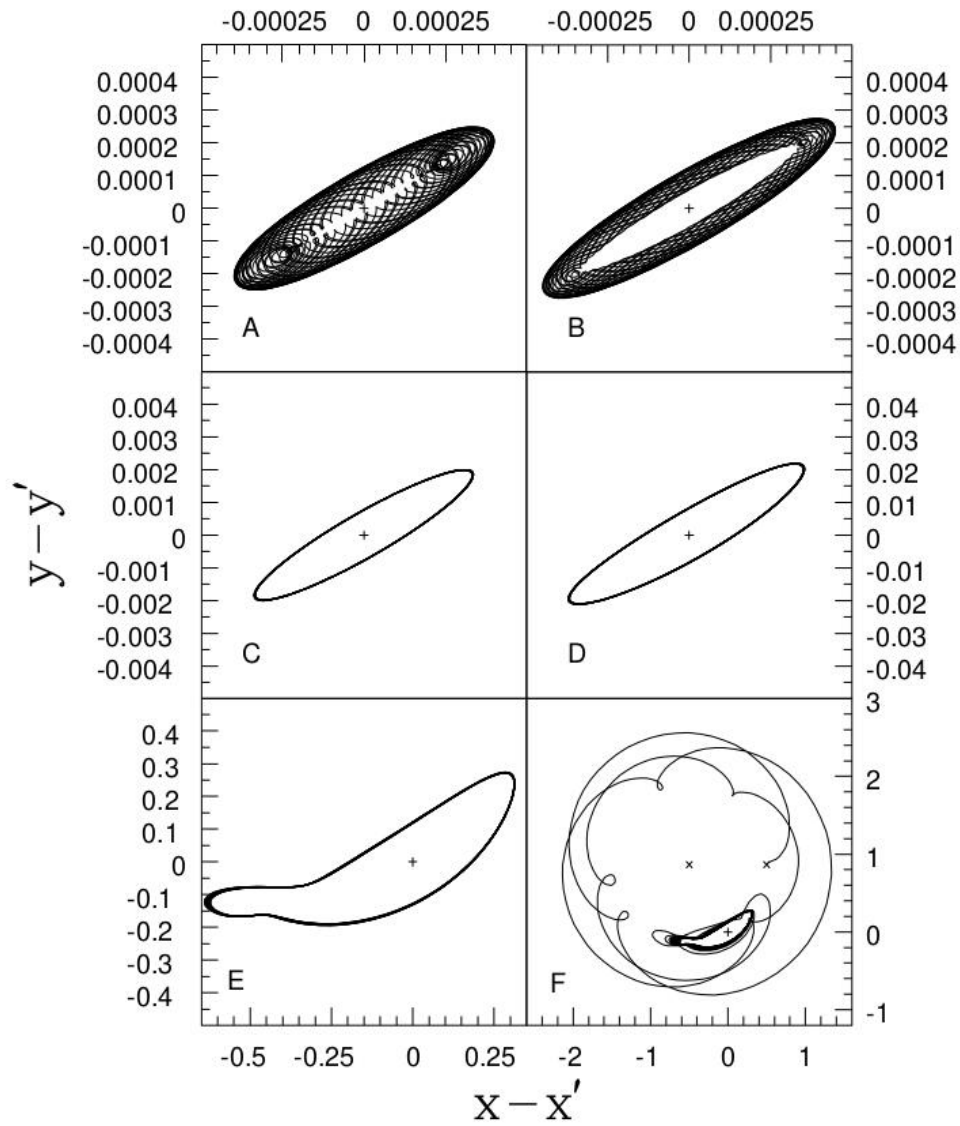


Figure 9: Numerical simulation of Case 5. Panel A: The first 100 orbital periods P of M_2 . Panel B: $t = 2000 P$ through $2100 P$. Panel C: $t = 20000 P$ through $20100 P$. Panel D: $t = 40000 P$ through $40100 P$. Panel E: $t = 60000 P$ through $60100 P$. Panel F: $t = 60100 P$ through $60333 P$. $x - x'$ and $y - y'$ are the horizontal deviations from the leading equilateral Lagrange point L'_4 . Note different scales in each panel. In Panel F, the \times on the left-hand side marks the location of M_1 , while the \times on the right marks the location of M_2 . The plus signs in each panel mark the origin, at L'_5 .

8 Appendix: Generalized Tidal Formulation

Here we derive the form of the tidal forces on a body of mass m_o in a right-handed Cartesian coordinate system X, Y, Z , retaining dimensional units. First, we must consider the tidal potential.

8.1 Potential

To begin, we assume that m_o is approximately spherically symmetric, with surface radius R . Then to lowest degree in R , m_o experiences a tidal potential

$$V_1 = GM_1 R^2 r_1^{-3} [3 \cos^2(\theta_1) - 1]/2 \quad (84)$$

at its surface due to the primary M_1 , and an analogous tidal potential

$$V_2 = GM_2 R^2 r_2^{-3} [3 \cos^2(\theta_2) - 1]/2 \quad (85)$$

at its surface due to the secondary M_2 .

Here

$$r_1 = \sqrt{(X_1 - X_o)^2 + (Y_1 - Y_o)^2 + (Z_1 - Z_o)^2} \quad (86)$$

is the distance between the centers of m_o at (X_o, Y_o, Z_o) and of M_1 at (X_1, Y_1, Z_1) , while

$$r_2 = \sqrt{(X_2 - X_o)^2 + (Y_2 - Y_o)^2 + (Z_2 - Z_o)^2} \quad (87)$$

is the distance between the centers of m_o and of M_2 , at (X_2, Y_2, Z_2) . Similarly, θ_1 is the angular distance along the surface of m_o from the point nearest to M_1 , while θ_2 is the analogous angular distance from the sub- M_2 point.

Actually, Formulae (84) through (87) above apply to any number of massive bodies $M_1, M_2, M_3, \dots, M_N$, as desired. For our present purposes, we confine ourselves to just M_1 and M_2 in the following; but our methods can readily be generalized for N-body applications.

Each of the tidal potentials V_1 and V_2 from Formulae (84) and (85) raises a bulge on the surface of m_o , of height hV_1/g and hV_2/g , respectively. Here $g = Gm_o/R^2$ is the acceleration of gravity on the surface of m_o , while h is a dimensionless constant depending on the internal structure of m_o , called its height Love number of the second degree (usually written h_2). For large, homogeneous fluid bodies, $h = 5/2$; but for a small solid object, h is smaller and proportional to its squared radius R^2 , all else being equal.

However, due to dissipation of the energy of deformation in the body of m_o , the tidal bulges do not align exactly with the peaks of the tidal potentials V_1 or V_2 , but rather with the *lagged* potentials V'_1 and V'_2 ; these are equal to V_1 and V_2 at the surface of m_o , but at a certain time $t - \tau$ *before* the current time t (somewhat analogous to the retarded potential of electrodynamics).

These lagged potentials can be written as

$$V' \approx GMR^2 r'^{-3} [3 \cos^2(\theta') - 1]/2, \quad (88)$$

where V' , r' , θ' , and M all are subscripted 1, as in Formula (84); or else they all are subscripted 2, as in Formula (85). Here r' is the distance between m_o and the tide-raising body M at the previous time $t - \tau$, while θ' is the angular distance along the surface of m_o from the location of the sub-perturber point at the previous time $t - \tau$.

It is common in many applications to replace τ with $P/(2\pi Q)$, where P is the period of the tides and Q is a dimensionless parameter known as the tidal "quality factor". Note that the dimensionless value of τ is just $1/Q$. For example, the tidal time lag τ is on the order of ten minutes for semi-diurnal tides ($P \approx 12$ hours) in the Earth, mostly due to the oceans; then the dimensionless value of τ is on the order of 0.1, so $Q \approx 10$. Using the same Q for annual tides ($P \approx 1$ year) would give $\tau \approx 5$ days.

Assuming that $Q \gg 1$, or equivalently, that τ is short compared to the tidal periods of interest (the “weak friction” approximation), then the lagged distance can be approximated as $r' \approx r - \dot{r}\tau$, while the lagged angular distance can be approximated as $\theta' \approx \theta - \dot{\theta}\tau$, both to first degree in τ .

Strictly speaking, the above expansion is formally appropriate only when the time lag τ is a constant, independent of the period P ; this corresponds to “viscous”-type tides, where the quality factor Q is directly proportional to P . However, the above treatment is questionable if τ depends on period (as in “constant- Q ” tides, where τ is directly proportional to P , more analogous to friction between solids). Still worse, if τ and Q depend on the amplitude of the tides, the tides are not even linear, and different components cannot simply be added together.

Assuming that the tides are linear, each tidal bulge generates its own quadrupole (inverse cube) potential

$$W = kV'R^3/r_o^3. \quad (89)$$

Here r_o is the distance of the field point from the center of m_o , while k is another dimensionless constant depending on the internal structure of m_o , called its potential Love number of the second degree (usually written k_2); k_2 is also known to astrophysicists as the “apsidal motion constant” (e.g., Alexander, 1973). For large, homogeneous fluid bodies, $k = 3/2$; but for a small solid object, k is smaller and proportional to its squared radius R^2 , like the height Love number h .

8.2 Forces

The quadrupole potentials W_1 and W_2 from Formula (89) above are responsible for the tidal forces and torques between m_o and the tide-raising bodies. The lag terms involving $\dot{r}\tau$ and $\dot{\theta}\tau$ in Formula (88) for V' are the reasons why those tidal forces and torques are not conservative in general.

For convenience, we decompose the forces into radial and transverse components. For example, the quadrupole potential W exerts a radial force of strength

$$m\partial W/\partial r_o = -3mkV'R^3/r_o^4 = -3kGMmR^5r'^{-3}r_o^{-4}[3\cos^2(\theta') - 1]/2, \quad (90)$$

as well as a *transverse* force of strength

$$mr_o^{-1}\partial W/\partial \theta' = -3kGMmR^5r'^{-3}r_o^{-4}\sin(\theta')\cos\theta', \quad (91)$$

on any mass m at a distance r_o from m_o , and at an angular distance θ' from the axis of the tidal bulge.

If the perturbed body m is located at (X_m, Y_m, Z_m) , the radial force on m from Formula (90) is directed along $\mathbf{r}_o = (X_m - X_o, Y_m - Y_o, Z_m - Z_o)$, the vector location of m relative to the center of m_o ; but the transverse force from Formula (91) above lies in the direction of the part of $\mathbf{r}_o - \mathbf{r}'$ perpendicular to \mathbf{r}_o , where \mathbf{r}' is the time-lagged vector location of the tide-raising body relative to m_o . By Newton’s third law, m exerts an equal force on m_o , but in the opposite direction.

It is interesting to note that in an equilateral configuration where θ_1 and θ_2 are each 60° , the radial force of M_1 on the tidal bulge induced in m_o by M_2 turns out to be positive, corresponding to a slight repulsion; and the same applies to the radial force of M_2 on the tidal bulge induced in m_o by M_1 .

In order to evaluate $\cos\theta'$ in Formulae (90) and (91), we take the scalar product of the unit vectors (designated by carats) in the directions of \mathbf{r}_o and \mathbf{r}' :

$$\cos\theta' = \hat{r}_o \bullet \hat{r}' = \frac{\mathbf{r}_o \bullet \mathbf{r}'}{r_o r'}. \quad (92)$$

However, Formula (92) above is not adequate to determine θ' when it is small, such as when the tide-raising and perturbed bodies are one and the same. Therefore we use the *cross* product of \hat{r}_o and \hat{r}' to evaluate $\sin\theta'$ in Formula (91):

$$\sin\theta' = |\hat{r}_o \times \hat{r}'| = \frac{|\mathbf{r}_o \times \mathbf{r}'|}{r_o r'}. \quad (93)$$

Now we separate \mathbf{r}' itself into radial and transverse vectors, respectively parallel and perpendicular to \mathbf{r}_o . The radial part of \mathbf{r}' is

$$\mathbf{r}'_R = \hat{r}_o r' \cos \theta' = \hat{r}_o (\mathbf{r}_o \bullet \mathbf{r}') / r_o = \mathbf{r}_o (\mathbf{r}_o \bullet \mathbf{r}') / r_o^2. \quad (94)$$

Then subtracting this radial part from \mathbf{r}' leaves the transverse part of \mathbf{r}' :

$$\mathbf{r}'_T = \mathbf{r}' - \mathbf{r}'_R = \mathbf{r}' - (\mathbf{r}_o \bullet \mathbf{r}') \mathbf{r}_o / r_o^2. \quad (95)$$

It is easy to verify that \mathbf{r}'_T above is orthogonal to \mathbf{r}_o : $\mathbf{r}_o \bullet \mathbf{r}'_T = \mathbf{r}_o \bullet [\mathbf{r}' - \mathbf{r}_o (\mathbf{r}_o \bullet \mathbf{r}') / r_o^2] = \mathbf{r}_o \bullet \mathbf{r}' - (\mathbf{r}_o \bullet \mathbf{r}_o) (\mathbf{r}_o \bullet \mathbf{r}') / r_o^2 = \mathbf{r}_o \bullet \mathbf{r}' - \mathbf{r}_o \bullet \mathbf{r}' = 0$.

This decomposition of \mathbf{r}' into radial and transverse parts makes it easier to evaluate the cross product in Formula (93):

$$\sin \theta' = \frac{|\mathbf{r}_o \times \mathbf{r}'|}{r_o r'} = \frac{|\mathbf{r}_o \times (\mathbf{r}'_R + \mathbf{r}'_T)|}{r_o r'} = \frac{|(\mathbf{r}_o \times \mathbf{r}'_R) + (\mathbf{r}_o \times \mathbf{r}'_T)|}{r_o r'} = \frac{|\mathbf{0} + \mathbf{r}_o \times \mathbf{r}'_T|}{r_o r'} = \frac{|\mathbf{r}_o| |\mathbf{r}'_T|}{r_o r'} = |\mathbf{r}'_T| / r'. \quad (96)$$

Now we can write the radial part of the tidal force on m_o as

$$\mathbf{F}_R = 3kGMmR^5 r'^{-5} r_o^{-7} [3(\mathbf{r}_o \bullet \mathbf{r}')^2 - r_o^2 r'^2] \mathbf{r}_o / 2 \quad (97)$$

from Formulae (90) and (92), and the transverse part of the tidal force on m_o as

$$\mathbf{F}_T = -3kGMmR^5 r'^{-5} r_o^{-5} [\mathbf{r}_o \bullet \mathbf{r}'] \mathbf{r}'_T = -3kGMmR^5 r'^{-5} r_o^{-7} [\mathbf{r}_o \bullet \mathbf{r}'] [r_o^2 \mathbf{r}' - (\mathbf{r}_o \bullet \mathbf{r}') \mathbf{r}_o] \quad (98)$$

from Formulae (91) and (95). Finally, re-combining these gives the total tidal force on m_o :

$$\mathbf{F} = \mathbf{F}_R + \mathbf{F}_T = 3kGMmR^5 r'^{-5} r_o^{-7} \{ [5(\mathbf{r}_o \bullet \mathbf{r}')^2 - r_o^2 r'^2] \mathbf{r}_o / 2 - [\mathbf{r}_o \bullet \mathbf{r}'] r_o^2 \mathbf{r}' \}. \quad (99)$$

8.3 Lagged location

The next issue is to evaluate \mathbf{r}' , the effective value of \mathbf{r} at a time $t - \tau$ before the current time t . If m_o were not spinning at all, we could approximate $\mathbf{r}' \approx \mathbf{r} - \dot{\mathbf{r}}\tau$, to first degree in τ . However, if m_o is spinning rigidly with angular velocity vector $\boldsymbol{\omega}$, its rotation drags the tidal bulge away from the sub-perturber point, as if the tide-raising body M had an additional transverse velocity

$$\boldsymbol{\omega} = \mathbf{r} \times \boldsymbol{\omega} \quad (100)$$

in a reference frame fixed in the body of m_o .

Note that $\boldsymbol{\omega}$ is orthogonal to \mathbf{r} , so $\mathbf{r} \bullet \boldsymbol{\omega} = 0$. Then we may approximate

$$\mathbf{r}' \approx \mathbf{r} - [\dot{\mathbf{r}} + \boldsymbol{\omega}] \tau, \quad (101)$$

and

$$r'^2 = \mathbf{r}' \bullet \mathbf{r}' \approx r^2 - 2[\mathbf{r} \bullet \dot{\mathbf{r}}] \tau = r^2 - 2r\dot{r}\tau, \quad (102)$$

both to first degree in τ .

In Formula (102) above, we have replaced $\mathbf{r} \bullet \dot{\mathbf{r}}$ with $\frac{d}{dt}(\mathbf{r} \bullet \mathbf{r}) / 2 = \frac{d}{dt} r^2 / 2 = r\dot{r}$. The time derivative of the distance r appearing in Formula (102) is

$$\dot{r} = ([X - X_o][\dot{X} - \dot{X}_o] + [Y - Y_o][\dot{Y} - \dot{Y}_o] + [Z - Z_o][\dot{Z} - \dot{Z}_o]) / r, \quad (103)$$

from Formula (84) or (85). Note that Formula (103) above for \dot{r} is not the same as the speed $|\dot{\mathbf{r}}| = \sqrt{[\dot{X} - \dot{X}_o]^2 + [\dot{Y} - \dot{Y}_o]^2 + [\dot{Z} - \dot{Z}_o]^2}$ of the tide-raising body M relative to m_o ; instead, \dot{r} is just the *radial component* of its vector velocity $\dot{\mathbf{r}}$.

8.4 Primary

Now consider the case when the primary M_1 is both the tide-raising body M and the perturbed body m . Then $\mathbf{r}_0 = \mathbf{r} = \mathbf{r}_1$, $\mathbf{r}' = \mathbf{r}'_1$, $\mathbf{s} = \mathbf{s}_1$, and Formula (59) for the tidal force on m_o becomes

$$\begin{aligned}
\mathbf{F}_{11} &= 3kGM_1^2 R^5 r_1'^{-5} r_1^{-7} \{ [5(\mathbf{r}_1 \bullet \mathbf{r}'_1)^2 - r_1'^2 r_1'^2] \mathbf{r}_1 / 2 - [\mathbf{r}_1 \bullet \mathbf{r}'_1] r_1'^2 \mathbf{r}'_1 \} \\
&\approx 3kGM_1^2 R^5 r_1'^{-5} r_1^{-7} \{ [5r_1^4 / 2 - 5r_1^2 (\mathbf{r}_1 \bullet \dot{\mathbf{r}}_1) \tau - r_1^4 / 2 + r_1^2 (\mathbf{r}_1 \bullet \dot{\mathbf{r}}_1) \tau] \mathbf{r}_1 - [\mathbf{r}_1 \bullet \mathbf{r}'_1] r_1'^2 \mathbf{r}'_1 \} \\
&= 3kGM_1^2 R^5 r_1'^{-5} r_1^{-5} \{ [2r_1^2 - 4(\mathbf{r}_1 \bullet \dot{\mathbf{r}}_1) \tau] \mathbf{r}_1 - [\mathbf{r}_1 \bullet \mathbf{r}'_1] \mathbf{r}'_1 \} \\
&\approx 3kGM_1^2 R^5 r_1'^{-5} r_1^{-5} \{ [2r_1^2 - 4(\mathbf{r}_1 \bullet \dot{\mathbf{r}}_1) \tau] \mathbf{r}_1 - [r_1^2 - (\mathbf{r}_1 \bullet \dot{\mathbf{r}}_1) \tau] [\mathbf{r}_1 - (\dot{\mathbf{r}}_1 + \boldsymbol{\omega}_1) \tau] \} \\
&\approx 3kGM_1^2 R^5 r_1'^{-5} r_1^{-5} \{ [r_1^2 - 3(\mathbf{r}_1 \bullet \dot{\mathbf{r}}_1) \tau] \mathbf{r}_1 + r_1^2 [\dot{\mathbf{r}}_1 + \boldsymbol{\omega}_1] \tau \} \\
&\approx 3kGM_1^2 R^5 r_1'^{-5} r_1^{-5} \{ [r_1^2 - 3r_1 \dot{r}_1 \tau] \mathbf{r}_1 + r_1^2 [\dot{\mathbf{r}}_1 + \boldsymbol{\omega}_1] \tau \} \\
&\approx 3kGM_1^2 R^5 r_1'^{-5} r_1^{-3} \{ [1 - 3\dot{r}_1 \tau / r_1] \mathbf{r}_1 + [\dot{\mathbf{r}}_1 + \boldsymbol{\omega}_1] \tau \} \\
&\approx 3kGM_1^2 R^5 r_1^{-8} [1 + 5\dot{r}_1 \tau / r_1] \{ [1 - 3\dot{r}_1 \tau / r_1] \mathbf{r}_1 + [\dot{\mathbf{r}}_1 + \boldsymbol{\omega}_1] \tau \} \\
&\approx 3kGM_1^2 R^5 r_1^{-8} \{ [1 + 2\dot{r}_1 \tau / r_1] \mathbf{r}_1 + [\dot{\mathbf{r}}_1 + \boldsymbol{\omega}_1] \tau \}, \tag{104}
\end{aligned}$$

again to first degree in τ .

The first term inside the braces $\{ \}$ in Formula (104) above represents the enhanced radial attraction of M_1 on m_o due to its tidal bulge, independent of dissipation or of the time lag τ . The three remaining terms all are proportional to τ ; the second term $+2\dot{r}_1 \tau \mathbf{r}_1 / r_1$ gives a small modification of the first term due to just the radial component of $\dot{\mathbf{r}}_1$. The third term $+\dot{\mathbf{r}}_1 \tau$ represents an additional small force on m_o proportional to $\dot{\mathbf{r}}_1$, while the last term $+\boldsymbol{\omega}_1 \tau$ gives an additional transverse force on m_o due to its rotation. It is gratifying to verify that the latter three terms are equivalent to Formula (5) of Mignard (1979) in the two-body case.

8.5 Secondary

In a two-body problem, \mathbf{F}_{11} above would be the only tidal force to include; but a three-body problem introduces three more tidal forces to consider. Of course, the attraction of the secondary M_2 on the tidal bulge it raises in m_o also produces its own force

$$\mathbf{F}_{22} \approx 3kGM_2^2 R^5 r_2'^{-8} \{ [1 + 2\dot{r}_2 \tau / r_2] \mathbf{r}_2 + [\dot{\mathbf{r}}_2 + \boldsymbol{\omega}_2] \tau \} \tag{105}$$

on m_o , analogous to Formula (104) for \mathbf{F}_{11} .

Note that the secondary force \mathbf{F}_{22} is weaker than the corresponding primary force \mathbf{F}_{11} by a factor of $(M_2/M_1)^2$, all else being equal. However, there are also two cross-interactions to consider as well, each of intermediate order M_2/M_1 .

8.6 Mixed

Now consider the case when the tide-raising body M is the primary M_1 , but the perturbed body m is the secondary M_2 . Then $\mathbf{r}_o = \mathbf{r}_2$, but $\mathbf{r} = \mathbf{r}_1$, $\mathbf{r}' = \mathbf{r}'_1$, $\boldsymbol{\omega} = \boldsymbol{\omega}_1$, and Formula (99) for the tidal force on m_o becomes

$$\begin{aligned}
\mathbf{F}_{12} &= 3kGM_1 M_2 R^5 r_1'^{-5} r_2^{-7} \{ [5(\mathbf{r}_2 \bullet \mathbf{r}'_1)^2 - r_2'^2 r_1'^2] \mathbf{r}_2 / 2 - [\mathbf{r}_2 \bullet \mathbf{r}'_1] r_2'^2 \mathbf{r}'_1 \} \\
&\approx 3kGM_1 M_2 R^5 r_1'^{-5} r_2^{-7} \{ [5(\mathbf{r}_2 \bullet [\mathbf{r}_1 - (\dot{\mathbf{r}}_1 + \boldsymbol{\omega}_1) \tau])^2 - r_2'^2 [r_1'^2 - 2(\mathbf{r}_1 \bullet \dot{\mathbf{r}}_1) \tau] \mathbf{r}_2 / 2 \\
&\quad - [\mathbf{r}_2 \bullet (\mathbf{r}_1 - [\dot{\mathbf{r}}_1 + \mathbf{s}_1] \tau)] r_2'^2 [\mathbf{r}_1 - (\dot{\mathbf{r}}_1 + \boldsymbol{\omega}_1) \tau] \} \\
&\approx 3kGM_1 M_2 R^5 r_1'^{-5} r_2^{-7} \{ [5(\mathbf{r}_2 \bullet \mathbf{r}_1)^2 - 10(\mathbf{r}_2 \bullet \mathbf{r}_1) [\mathbf{r}_2 \bullet (\dot{\mathbf{r}}_1 + \boldsymbol{\omega}_1) \tau - r_1'^2 r_2^2 + 2r_2'^2 (\mathbf{r}_1 \bullet \dot{\mathbf{r}}_1) \tau] \mathbf{r}_2 / 2
\end{aligned}$$

$$\begin{aligned}
& -[\mathbf{r}_2 \bullet (\mathbf{r}_1 - [\dot{\mathbf{r}}_1 + \mathbf{s}_1] \tau)] r_2^2 \mathbf{r}_1 + [\mathbf{r}_2 \bullet \mathbf{r}_1] r_2^2 (\dot{\mathbf{r}}_1 + \boldsymbol{\omega}_1) \tau \\
\approx & 3kGM_1 M_2 R^5 r_1^{-5} r_2^{-7} [1 + 5\dot{r}_1 \tau / r_1] \{ [5(\mathbf{r}_2 \bullet \mathbf{r}_1)^2 - 10(\mathbf{r}_2 \bullet \mathbf{r}_1) [\mathbf{r}_2 \bullet (\dot{\mathbf{r}}_1 + \boldsymbol{\omega}_1)] \tau - r_1^2 r_2^2 + 2r_2^2 r_1 \dot{r}_1 \tau] \mathbf{r}_2 / 2 \\
& - [\mathbf{r}_2 \bullet (\mathbf{r}_1 - [\dot{\mathbf{r}}_1 + \mathbf{s}_1] \tau)] r_2^2 \mathbf{r}_1 + [\mathbf{r}_2 \bullet \mathbf{r}_1] r_2^2 (\dot{\mathbf{r}}_1 + \boldsymbol{\omega}_1) \tau \\
\approx & 3kGM_1 M_2 R^5 r_1^{-5} r_2^{-7} \{ [5(\mathbf{r}_2 \bullet \mathbf{r}_1)^2 - 10(\mathbf{r}_2 \bullet \mathbf{r}_1) [\mathbf{r}_2 \bullet (\dot{\mathbf{r}}_1 + \boldsymbol{\omega}_1)] \tau - r_1^2 r_2^2 + 2r_2^2 r_1 \dot{r}_1 \tau] \mathbf{r}_2 / 2 \\
& - [\mathbf{r}_2 \bullet (\mathbf{r}_1 - [\dot{\mathbf{r}}_1 + \mathbf{s}_1] \tau)] r_2^2 \mathbf{r}_1 + [\mathbf{r}_2 \bullet \mathbf{r}_1] r_2^2 (\dot{\mathbf{r}}_1 + \boldsymbol{\omega}_1) \tau + 5 \{ [5(\mathbf{r}_2 \bullet \mathbf{r}_1)^2 - r_1^2 r_2^2] \mathbf{r}_2 / 2 - [\mathbf{r}_2 \bullet \mathbf{r}_1] r_2^2 \mathbf{r}_1 \} \dot{r}_1 \tau / r_1 \} \\
= & 3kGM_1 M_2 R^5 r_1^{-5} r_2^{-7} \{ [5(\mathbf{r}_2 \bullet \mathbf{r}_1)^2 - 10(\mathbf{r}_2 \bullet \mathbf{r}_1) [\mathbf{r}_2 \bullet (\dot{\mathbf{r}}_1 + \boldsymbol{\omega}_1)] \tau - r_1^2 r_2^2 - 3r_2^2 r_1 \dot{r}_1 \tau] \mathbf{r}_2 / 2 \\
& - [\mathbf{r}_2 \bullet (\mathbf{r}_1 - [\dot{\mathbf{r}}_1 + \mathbf{s}_1] \tau)] r_2^2 \mathbf{r}_1 + [\mathbf{r}_2 \bullet \mathbf{r}_1] r_2^2 (\dot{\mathbf{r}}_1 + \boldsymbol{\omega}_1) \tau + 5 [5(\mathbf{r}_2 \bullet \mathbf{r}_1)^2 \mathbf{r}_2 / 2 - (\mathbf{r}_2 \bullet \mathbf{r}_1) r_2^2 \mathbf{r}_1] \dot{r}_1 \tau / r_1 \}, \quad (106)
\end{aligned}$$

again to first degree in τ .

Formula (106) above is equivalent to the intermediate result (4.3) of Mignard (1979), except that his formula does not include the terms without τ . It also comes as some relief to verify that Formula (106) reduces to Formula (104) or (105) when M_1 and M_2 are the same object. In the case when the tide-raising body M is the secondary M_2 , but the perturbed body m is the primary M_1 , the tidal force \mathbf{F}_{21} on m_o is found by swapping the subscripts 1 and 2 in Formula (106) above.

Finally, the net tidal force on m_o is just the sum of the four individual terms:

$$\mathbf{F} = \mathbf{F}_{11} + \mathbf{F}_{12} + \mathbf{F}_{21} + \mathbf{F}_{22}. \quad (107)$$

Unfortunately, adding \mathbf{F}_{12} and \mathbf{F}_{21} together does not seem to lead to any important simplifications.

ACKNOWLEDGEMENTS

Support for this work was provided by NASA's PSD ISFM program. We thank two anonymous reviewers for their service and helpful suggestions, as well as Jeff Cuzzi and José Alvarelos for constructive critiques of a draft.

REFERENCES

- Alexander, M. E., 1973. The weak friction approximation and tidal evolution in close binary systems. *Astrophysics and Space Science* **23**, 459–510.
- Beaugé, C., Zs. Sándor, B. Érdi, and Á. Süli, 2007. Co-orbital terrestrial planets in exoplanetary systems: a formation scenario. *Astronomy & Astrophysics* **463**, 359–367.
- Caton, D. B., S. A. Davis, and B. D. Walls, 1999. A search for Trojan planets: A novel approach for looking for transits of extrasolar planets (abstract). *B.A.A.S.* **31**, 1534.
- Caudal, G. V., 2013. The role of tidal torques on the evolution of the system of Saturn's co-orbital satellites Janus and Epimetheus. *Icarus* **223**, 733–740.
- Colombo, G., D. A. Lautman, and I. I. Shapiro, 1966. The Earth's dust belt: Fact or fiction? 2. Gravitational focussing and Jacobi capture. *JGR* **71**, 5705–5717.
- Couturier, J., P. Robutel, and A. C. M. Correia, 2021. An analytical model for tidal evolution in co-orbital systems. I. Application to exoplanets. *Cel. Mech. Dyn. Astron.* 133:37.
- Couturier, J., P. Robutel, and A. C. M. Correia, 2022. Dynamics of co-orbital exoplanets in a first order resonance chain with tidal dissipation. Submitted to *Astronomy & Astrophysics*. arXiv:2204.08074v1.
- Ćuk, M., D. P. Hamilton, and M. J. Holman, 2012. Long-term stability of horseshoe orbits. *M.N.R.A.S.* **426**, 3051–3056.
- Davis, S. A., D. B. Caton, K. A. Klutz, K. D. Wohlman, R. J. Stamilio, and K. B. Hix, 2001. The search for extrasolar Trojan planets: An update (abstract). *B.A.A.S.* **33**, 1303.
- de la Barre, C. M., W. M. Kaula, and F. Varadi, 1996. A study of orbits near Saturn's triangular Lagrangian points. *Icarus* **121**, 88–113.
- Dobrovolskis, A. R., 2007. Spin states and climates of eccentric exoplanets. *Icarus* **192**, 1–23.
- Dobrovolskis, A. R., 2012. Counter-orbitals: another class of co-orbitals. *AAS Division for Planetary Sciences Meeting* **44**, abstract 112.22.
- Dobrovolskis, A. R., 2013. Effects of Trojan exoplanets on the reflex motions of their parent stars. *Icarus* **26**, 1635–1641.
- Dobrovolskis, A. R., 2015. Radial velocities of stars with multiple co-orbital planets. *Astrophysics and Space Science* **356**, 241–249. See also arXiv :1404.5377v1.
- Ferraz-Mello, F., 2022. On tides and exoplanets. In *Multi-scale dynamics of space objects*. Proceedings of IAU Symposium No. 364, ed. A. Celletti, C. Beaugé, C. Galeş, and A. Lemaitre. arXiv:2111.01984v2.
- Ford, E. B., and B. S. Gaudi, 2006. Observational constraints on Trojans of transiting extrasolar planets. *Ap. J. Letters* **652**, L137–L140.
- Ford, E. B., and M. J. Holman, 2007. Using transit timing observations to search for Trojans of transiting extrasolar planets. *Ap. J. Letters* **664**, L51–L54.
- Giuppone, C. A., P. Benítez-Llambay, and C. Beaugé, 2012. Origin and detectability of co-orbital planets from radial velocity data. *M.N.R.A.S.* **421**, 356–368.
- Goździewski, K., and M. Konacki, 2006. Trojan pairs in the HD128311 and HD82943 planetary systems? *Ap. J* **647**, 573–586.
- Greenberg, R. (1978). Orbital resonance in a dissipative medium. *Icarus* **48**, 12–22.
- Guerrero, N. M., and 104 co-authors, 2021. The TESS objects of interest catalog from the TESS prime mission. *Ap. J. Supplements* **254**, 39.
- H'énnon, M., and M. Guyot, 1970. Stability of periodic orbits in the restricted problem. Pp. 349–374 in *Periodic Orbits, Stability and Resonances*, ed. G. E. O. Giacaglia. Dordrecht-Holland: D. Reidel Publishing Company.
- Hippke, M., and D. Angerhausen, 2015. A statistical search for a population of exo-Trojans in the Kepler data set. *Ap. J.* **811**:1.
- Hut, P., 1981. Tidal evolution in close binary systems. *Astronomy & Astrophysics* **99**, 126–140.
- Ingersoll, A. P., and A. R. Dobrovolskis, 1978. Venus' rotation and atmospheric tides. *Nature* **275**, 37–38.
- Janson, M., 2013. A systematic search for Trojan planets in the Kepler data. *Ap. J.* **774**:156.
- Jeffreys, H., 1929. *The Earth*, 2d ed. Cambridge U. Press.
- Kipping, D., 2020. An independent analysis of the six recently claimed exomoon candidates. *Ap. J. Letters* **900**: L44.

- Lainey, V., and 10 co-authors, 2020. Resonance locking in giant planets indicated by the rapid orbital expansion of Titan. *Nature Astronomy* **4**, 1053–1058.
- Laughlin, G., and J. E. Chambers, 2002. Extrasolar Trojans: The viability and detectability of planets in the 1:1 resonance. *Astron. J.* **124**, 592–600.
- Leleu, A., G. A. L. Coleman, and S. Ataiee, 2019. Stability of the co-orbital resonance under dissipation. Application to its evolution in protoplanetary discs. *Astronomy & Astrophysics* **631**, A6.
- Lillo-Box, J., and 7 co-authors, 2018a. The TROY project: Searching for co-orbital bodies to known planets. I. Project goals and first results from archival radial velocity. *Astronomy & Astrophysics* **609**, A96.
- Lillo-Box, J., and 12 co-authors, 2018b. The TROY project: Multi-technique constraints on exotrojans in nine planetary systems. *Astronomy & Astrophysics* **618**, A42.
- Lissauer, J. J., P. Goldreich, and S. Tremaine, 1985. Evolution of the Janus-Epimetheus coorbital resonance due to torques from Saturn's rings. *Icarus* **64**, 425–434.
- Lissauer, J. J., and 24 co-authors, 2011. Architecture and dynamics of *Kepler*'s candidate multiple transiting planet systems. *Ap. J.* **197**:8.
- Madhusudhan, N., and J. N. Winn, 2009. Empirical constraints on Trojan companions and orbital eccentricities in 25 transiting exoplanetary systems. *Ap. J.* **693**, 784–793.
- Mignard, F., 1979. The evolution of the lunar orbit revisited. I. *The Moon and the Planets* **20**, 301–315.
- Morais, M. H. N., and F. Namouni, 2013. Retrograde resonance in the planar three-body problem. *Cel. Mech. Dyn. Astron.* **125**, 91–106.
- Morais, M. H. N., and F. Namouni, 2016. A numerical investigation of coorbital stability and libration in three dimensions. *Cel. Mech. Dyn. Astron.* **125**, 91–106.
- Murray, C. D., 1994. Dynamical Effects of Drag in the Circular Restricted Three-Body Problem: I. Location and Stability of the Lagrangian Equilibrium Points. *Icarus* **112**, 465–484.
- Murray, C. D., and S. F. Dermott, 1999. *Solar System Dynamics*. Cambridge U. Press.
- Narita, N., *et al.*, 2007. Measurement of the Rossiter-McLaughlin effect in the transiting exoplanetary system TrES-1. *Pub. Astron. Soc. Japan* **59**, 763–770.
- Nauenberg, M., 2002. Stability and eccentricity for two planets in a 1:1 resonance, and their possible occurrence in extrasolar planetary systems. *Astron. J.* **124**, 2332–2338.
- Noyelles, B., J. Frouard, V. V. Makarov, and M. Efroimsky, 2014. Spin-orbit evolution of Mercury revisited. *Icarus* **241**, 26–44.
- Peale, S. J. (1993). The effect of the nebula on the Trojan precursors. *Icarus* **106**, 308–322.
- Press, W. H., S. A. Teukolsky, W. T. Vetterling, and B. P. Flannery, 1992. *Numerical Recipes in Fortran, Second Edition*. Cambridge U. Press.
- Rodríguez, A., C. A. Giuppone, and T. A. Michtchenko, 2013. Tidal evolution of close-in exoplanets in co-orbital configurations. *Cel. Mech. Dyn. Astron.* **117**, 59–74.
- Rowe, J. F., and 28 co-authors, 2014. Validation of *Kepler*'s multiple planet candidates. III. Light curve analysis and announcement of hundreds of new multi-planet systems. *Ap. J.* **784**, 45.
- Schuerman, D. (1980). The restricted three-body problem including radiation pressure. *Ap. J.* **238**, 337–322.
- Sheppard, S. S., and C. A. Trujillo, 2006. A thick cloud of Neptune Trojans and their colors. *Science* **313**, 511–514.
- Simmons, J. F. L., A. J. C. McDonald, and J. C. Brown, 1985. The restricted 3-body problem with radiation pressure. *Cel. Mech.* **35**, 145–187.
- Smith, A. M., and J. J. Lissauer, 2010. Orbital stability of systems of closely-spaced planets, II: configurations with coorbital planets. *Cel. Mech. Dyn. Astron.* **107**, 487–500.
- Wiegert, P., M. Connors, and C. Veillet, 2017. A retrograde co-orbital asteroid of Jupiter. *Nature* **543**, 687–689.
- Yoder, C. F., 1979. Notes on the origin of the Trojan asteroids. *Icarus* **40**, 341–344.
- Yoder, C. F., G. Colombo, S. P. Synnott, and K. A. Yoder, 1983. Theory of motion of Saturn's coorbiting satellites. *Icarus* **53**, 431–443.